Studying rotational dynamics of epichlorohydrin using a Timepix3 camera

by

Lana Chaleunrath-Pham

B.S., University of Mary Washington, 2023

A THESIS

submitted in partial fulfillment of the
requirements for the degree

MASTER OF SCIENCE

Department of Physics
College of Arts and Sciences

KANSAS STATE UNIVERSITY
Manhattan, Kansas

2025

Approved by:

Co-Major Professor
Vinod Kumarappan

Approved by:

Co-Major Professor
Daniel Rolles

Copyright

Abstract

In the field of ultrafast atomic, molecular, and optical physics, our goal is to study the dynamics of molecules. This thesis focuses on the rotational dynamics of chiral molecules induced by a laser pulse. Molecular rotations are quite fast, thus femtosecond laser pulses are used to drive the rotation as well as to monitor this rotation. A pump pulse is used to bring the molecule into motion and a probe pulse is used to break the molecule into ionic fragments. The momenta of these fragments are studied to understand the orientation and rotational motion of the initial molecule.

A significant portion of this thesis describes the implementation and synchronization of a Timepix3 camera into an existing experimental setup. Unlike a conventional camera which records the intensity of light onto pixels, the Timepix3 camera records the Time Of Arrival (TOA) of a light signal for each pixel and how long that signal stayed over a preset threshold (Time Over Threshold (TOT)). The pixels in the Timepix3 camera function independently from each other and collects the spatial coordinates, TOA, and TOT of an ion that lands on the detector. When used with a Velocity Map Imaging (VMI) spectrometer, the collected information can be used to find the mass over charge ratio and momenta of charged particles.

After the implementation of the Timepix3 camera, we investigated the rotations of the chiral molecule epichlorohydrin. The pump pulse induces rotational motion of the molecule's most polarizable axis, which causes the molecule to align and unalign itself with the polarization of the laser. The pump pulse also induces motion around the most polarizable axis. Simple symmetric molecules do not have a preference for the direction in which they rotate around this axis, but theory suggests that chiral molecules may have a preference. A portion of this thesis looks into how epichlorohydrin rotates and if it favors spinning in a particular direction, especially when comparing the left-handed and right-handed isomers.

Table of Contents

List of Figures

List of Tables

Acknowledgments

Huge thank you to one of my major professors, Dr. Vinod Kumarappan. For guiding me and teaching me so many things regarding this project and others. You are wonderful at explaining concepts and are always ready to answer any of my questions. It was with your help that I was able to complete this project as my master's thesis.

Another huge thank you to Dr. Daniel Rolles, my other major professor. Thank you for taking me into your research group and encouraging me to collaborate with Dr. Kumarappan's group and Dr. Phil Bucksbaum's group. And thank you for supporting me in prioritizing research during these years.

Thank you to the other collaborators of this project, Dr. Varun Makhija, Dr. Robert Jones, and Dr. Eric Wells for providing the theory and background knowledge needed for our experiment. It was great to have you all visit during the beamtime and provide feedback on the results. Thank you, Dr. Wells, for providing the Timepix3 camera.

Thank you to my coworkers in the lab: Diksha Ahlawat, Wyatt Jones, and Paige Lettow. Your presence during this beamtime not only resulted in the conclusions of this thesis, but it also kept the long work days fun. We were learning everything from the ground up and going through the trials and tribulations together.

Other coworkers I give thanks to are Kamrunnahar Kali and Ryan Cloughley. Thank you for helping me with parts of the data analysis and for lending an ear to my thoughts and presentations.

Thank you to the group members of Dr. Phil Bucksbaum's group: Ian Gabalski, Aaron Ghrist, and Eleanor Weckwerth. You all welcomed me into your lab and kindly shared how you collect data and your data analysis software. We improved our data analysis based on your shared code.

Thank you to Anbu Venkatachalam, Huynh Lam, John Searles, and Zane Phelps for help in maintaining the FLAME laser we used in our experiment and for the wealth of knowledge about the ins and outs of the lab.

Thank you to the technical staff: Chris Aikens, Justin Millette, Scott Chainey, and Vincent Needham. Without you all, the James R. Macdonald Lab would not be in operation. Thank you for quickly solving our physical/technical problems.

Thank you to Dr. Cosmin Blaga for reviewing my thesis and providing feedback along with my co-major professors.

Thank you to everyone in the K-State Physics Department for welcoming me into this community of scientists. I've met some amazing people in the two years here at K-State. Researchers who not only have an in-depth knowledge about the field, but who are also so kind and understanding to share that knowledge. There are many people from K-State that I'd call my friends. People who made my time here not just productive, but enjoyable. From boardgames in The Grounge to canoe trips at Tuttle Creek to home-cooked meals in colleagues' homes, I hold the time I've spent here very dearly.

Paige Lettow was supported by the National Science Foundation under Grant Nos. 2244539 (the Research Experience for Undergraduates program). The TimePix3 camera was purchased under Grant No. 2018286 (under Dr. Eric Wells). Participants from K-State were supported by the US Department of Energy under Grant No. DE-FG02-86ER13491.

Chapter 1

Introduction

The goal of this work is to integrate a Timepix3 camera into a Velocity Map Imaging (VMI) spectrometer setup and measure the rotational dynamics of a chiral molecule. The Timepix3 camera is developed by Amsterdam Scientific Instruments (ASI) as an efficient way to collect the position and timing information of particles from a detector at the end of the spectrometer. This chapter will give an introduction to what advantages a Timepix3 camera has as compared to traditional pixel cameras, while further into the thesis, I will discuss how the camera is integrated into our experimental setup in the James R Macdonald Laboratory (JRML). This chapter will also give a short overview of how we study the rotational dynamics of a molecule, and why we chose epichlorohydrin as our subject of investigation.

1.1 Introduction to Timepix3 Camera

A pump-probe scheme is used in our experiment; where an initial pump pulse impulsively rotates our molecule, and at a time delay later, a probe pulse induces ionization from the molecule. These ionic fragments land on a multichannel plate (MCP) detector, where their small charge gets amplified, and this signal reaches a part of a phosphor screen that briefly lights up. A lens collects this light signal and forms an image of the phosphor on the Timepix3 sensor. Fig 1.1 shows the combination of the MCP, phosphor, and Timepix3 camera.

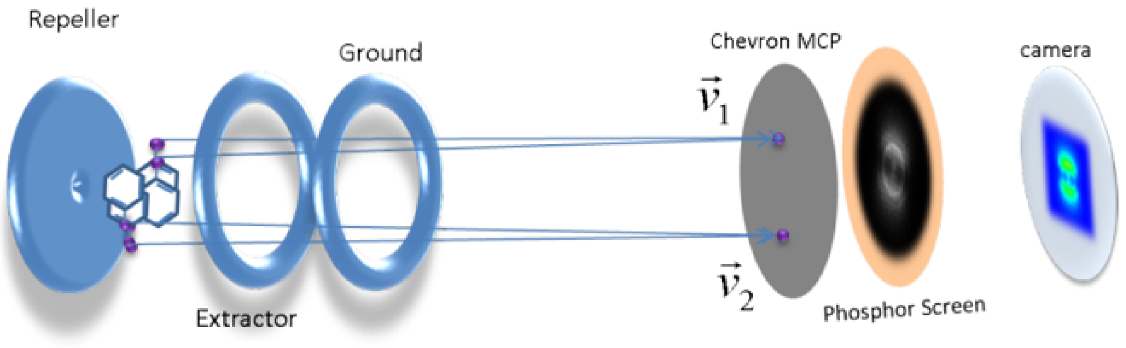

Figure 1.1: *Figure of spectrometer plates, MCP, phosphor, and Timepix3 camera combination. More details regarding this setup will be discussed in Chapter 3. Image is from Makhija's thesis*[1].

Unlike traditional cameras that capture information about every pixel in every frame, the Timepix3 camera only collects information about a particular pixel when the light signal that falls on it crosses a certain threshold. Therefore, rather than having many pixels of zero value recorded even when there is no signal detected, the Timepix3 only collects and reads out the pixels that witness a significant signal. Each pixel resets independently after a count with a short turnaround time. This makes the effective particle count rate of the Timepix3 much higher than traditional cameras, which is useful for experiments with high repetition rate lasers.

Each pixel of the Timepix3 camera records when it is triggered at the Time of Arrival (TOA), and it records the Time over Threshold (TOT). The threshold is to filter out unwanted noise, and the TOT acts as a proxy for the signal amplitude or the intensity. As shown in Fig 1.2, the longer the TOT, the brighter the pixel. An individual ion usually lights up several pixels as a cluster. Table 1.1 shows four values gathered from each pixel: TOA, TOT, and the spatial coordinates of the pixel, X and Y.

The Timepix3 camera has two advantages over a traditional charged-coupled device (CCD) or complementary metal oxide semiconductor (CMOS) camera. One advantage is the ability to capture the ToA and the TOT. Collecting each pixel's TOA and TOT timestamp, rather than frame-by-frame timings, allows nanosecond resolution[3,4]. This makes the Timepix3 camera a valuable asset when capturing the charged particles produced by lasers

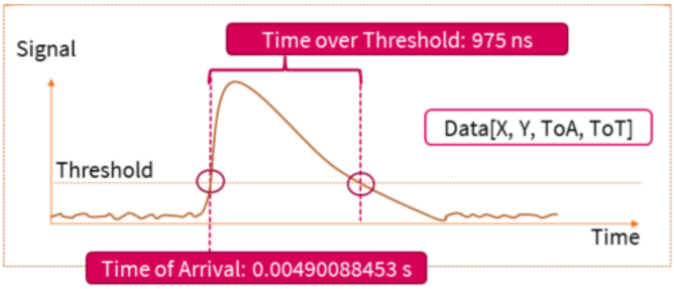

Figure 1.2: *Visual of the signal above a threshold and what the Timepix3 camera collects. Figure from Amsterdam Scientific Instruments' website*[2].

Time of Arrival (s)	Time Over Threshold (ns)	X (pixel number)	Y (pixel number)
0.001426789	50	396	112
0.001426780	50	400	112
0.001426730	175	399	115
0.001426767	75	396	113
0.001426760	150	400	113

Table 1.1: *Example events the Timepix3 collects.*

with high repetition rates.

Another advantage is that by recording the TOA for each pixel, the time of flight, and thus, the mass-to-charge ratio of each ion can be determined. This means that each ion species can be distinguished and recorded simultaneously, rather than needing to gate the ion detector for each specific ion fragment separately.

In our experimental setup, the ions of the studied molecule land on the MCP detector and phosphor screen that produces light flashes for the Timepix3 to see. Shown in Figure 1.3 is our Timepix3 camera near the detector connected to the target chamber. The Timepix3 collects simultaneous measurements of all ionic fragments of the molecule, which is advantageous for Velocity Map Imaging (VMI). The VMI spectrometer projects the transverse momenta of an ion to the positions of the detector. The information about the ion's mass-to-charge ratio and momentum in the direction towards the detector is found from the ion's Time of Flight (TOF). From this information gathered by the Timepix3 camera, we can thus find the initial orientation of the molecule. More details about how the Timepix3 is implemented into our experiment and the data acquisition process will be described in

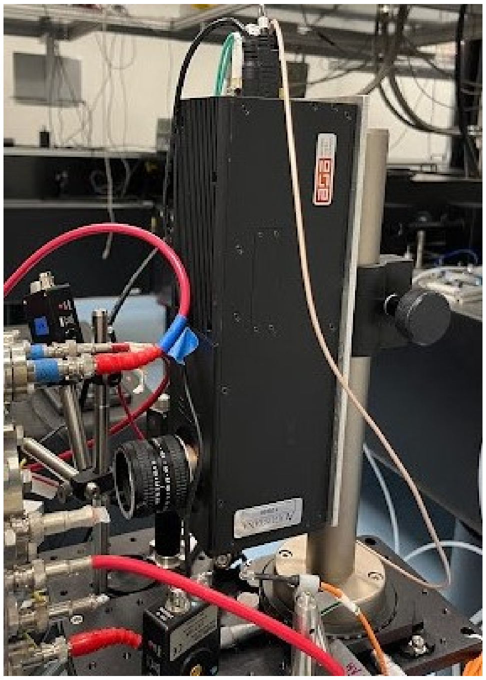

Figure 1.3: *Timepix3 camera mounted near the detector of the experimental setup*

Chapter 3 in this thesis.

1.2 Molecular Rotational Dynamics

Many studies are done to observe the properties and dynamics of molecules at an atomic level. Studying them provides the ability to predict how certain molecules will move and the ability to influence their behavior. In the ultrafast timescale of these motions, femtosecond pulses are used to discern the properties of these molecules[5]. In this timescale, everything that is larger than a molecule has near-zero motion. A glass of water spilling would look frozen in time, but the water molecules themselves would have some motion. The rotation, vibration, and electronic motion of these molecules can be studied using femtosecond pulses.

A molecule's interaction with other molecules or external fields depends on the orientation of that molecule. To consistently measure an interaction, we would want to align the molecule to be at a known orientation. We use femtosecond pulses to accomplish this. Chapter 2 will focus on the background theory needed to understand the rotational dynamics of our studied molecule.

The experiment that will be described in this thesis uses pairs of laser pulses: one to kick the molecule to start rotating, and another to break up the molecule into ionic fragments that get pulled to the detector. From the ion fragments, if the molecule fragments faster than it rotates, then the orientation and geometry of the molecule can be found by knowing the position and time of where the fragments land[6,7,8].

1.3 Introduction to Epichlorohydrin

The molecule that we are studying is epichlorohydrin (C_3H_5ClO), shown in Fig 1.4; a toxic liquid that is used in the production of epoxy resin[9]. Epichlorohydrin was chosen for several reasons. One reason is that it is a chiral, asymmetric top[10]. Asymmetric tops do not have a pattern to their motion when they rotate, unlike other tops that are symmetric. We are interested in seeing it's unpredictable motion as it rotates. Another reason is that it has two "marker" atoms (chlorine and oxygen), which we hope can be used to determine the 3D orientation of the molecule.

Figure 1.4: *The two isomers of epichlorohydrin. S-isomer on the left and R-isomer on the right. Gray atoms are carbon, white atoms are hydrogen, the green atom is chlorine, and the red atom is oxygen. Notice the difference in the oxygen being connected to the middle carbon and hydrogen on the isomers. Figure of molecule obtained from PubChem*[10].

To get the molecule to rotate, we use a laser pulse to interact with it. The electric field of the laser pulse forces charges of the molecule to shift and produce a dipole moment. This dipole then begins to align itself with the electric field or the polarization vector of the laser. This induces the rotational motion of the molecule. It is expected that the molecule will

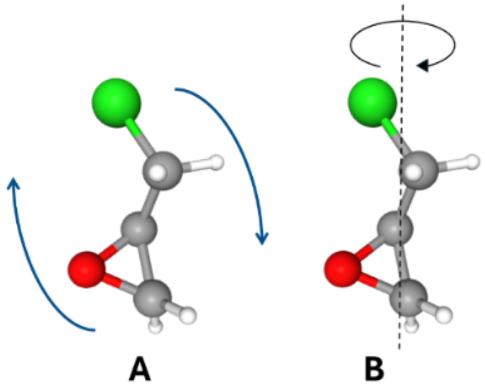

Figure 1.5: *Ways the molecule can rotate.* ***A*** *shows the motion of aligning with the polarization of the laser.* ***B*** *shows the motion around a molecular axis from the chlorine to the carbon. Figure of molecule provided by PubChem*[10].

mainly rotate in a way shown in Fig 1.5**A**, to align and unalign itself with the polarization of the laser. But because epichlorohydrin does not have a symmetry axis, the molecule also rotates around an axis shown in Fig 1.5**B**. The axis that runs from the chlorine (green atom) to the furthest carbon (gray atom) is the most polarizable. This axis has the most atoms closest to it, and is the axis that is used in defining how the molecule rotates. The laser pulse will cause epichlorohydrin to rotate in a manner that aligns this axis with the laser polarization; simultaneously, it also forces the molecule to spin around this molecular axis.

Epichlorohydrin is a chiral molecule with two mirror versions of each other, shown in Fig 1.4. While studying how the molecule orients itself as time progresses, the molecule may rotate in a different direction around the most polarizable axis, depending on which chiral isomer it is. Part of this experiment is seeing how one version of it rotates compared to the other mirrored version.

Chapter 2

Theory Fundamentals

This chapter first describes the frames and angles that will be used to describe how a molecule can rotate. It then considers how one can identify molecules as types of rigid rotors (or tops) based on their inertia tensor, and whether they can have periodic rotations depending on this categorization. This chapter is based, to a large extent, on the PhD theses of Varun Makhija[1] and Huynh Van Sa Lam[11].

2.1 Molecular Frame Coordinates

When discussing and interpreting ultrafast laser experiments on molecules, it is helpful to distinguish two different coordinate frames: the molecular frame and the laboratory frame. Each molecule has certain characteristics, such as the dipole moment and moments of inertia, which depend on its internal coordinate frame, which we call the molecular frame. The laboratory frame is defined by external experimental conditions such as the laser polarization direction, the laser propagation direction, and the direction of the spectrometer field. In most gas-phase experiments, molecules are, at least originally, randomly oriented in the laboratory frame.

The molecular frame is defined in Fig 2.1 with ethylene as an example, and the principal components of its moment of inertia determining the axis. Following standard convention,

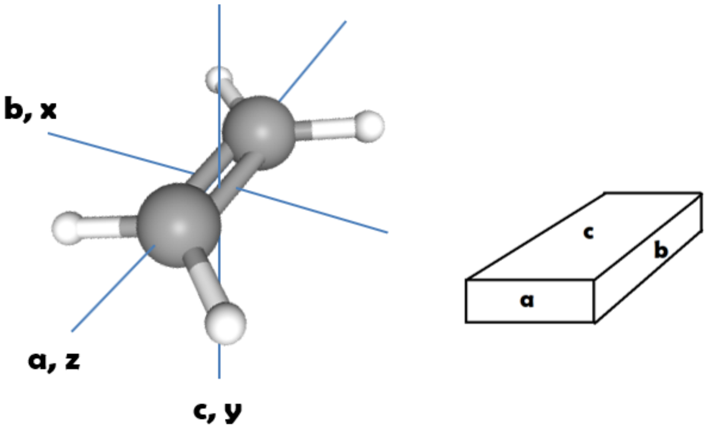

Figure 2.1: *Ethylene molecule in the molecular frame. Dark grey atoms are carbon atoms, and white atoms are hydrogen atoms. The principal axes are drawn and labeled a, b, and c. The rectangular box is a simplified form of ethylene with labels of the principal axes on the surfaces of the box. x, y, and z axes are assigned, with the axis with the highest symmetry (C-C axis) chosen as the z axis.*

the axis with the smallest moment of inertia is labeled a, the intermediate one b, and the largest one c. In the case of ethylene, we can coincide the a axis with the most polarizable z axis, and the c axis with the least polarizable y axis in the molecular frame. For other molecules, the choice of how to match these a, b, and c axes to x, y and z may be different.

In this free-particle situation, Eq 2.1 describes the Hamiltonian:

$$\begin{aligned} H &= \frac{J^2}{2I} \\ &= \frac{J_a^2}{2I_a} + \frac{J_b^2}{2I_b} + \frac{J_c^2}{2I_c} \\ &= AJ_a^2 + BJ_b^2 + CJ_c^2 \end{aligned} \tag{2.1}$$

where the kinetic energy term replaces the linear momentum with angular momentum J_i around each principal axis. A, B, and C are proportional to the fundamental frequencies of rotation around each principal axis. I_a, I_b, and I_c are the principal components of the moment of inertia tensor. We assume all the molecules in this thesis as rigid rotors.

Any molecule with three unequal principal moments of inertia ($I_a < I_b < I_c$), including ethylene, can be thought of as a box with unequal sides. If the molecule is set into rotation around principal axis m ($m = a, b$, or c) with angular momentum J, the rotational kinetic energy of the molecule would be $KE = I_m\omega^2/2 = J^2/2I_m$. Thus, $\omega = J/I_m$, implying that the box would spin fastest if the angular moment J is along the a axis and slowest if it is along the c axis. The box has the largest and smallest possible kinetic energies, respectively, in these two cases as well. Since both KE and J are conserved when there is no external torque, if the molecule starts along (or near) either of these axes, it must continue to do so. Thus, motion around these axes is stable. Motion around the b axis is not similarly constrained. The axis of rotation moves away from this axis, and the motion is unstable and non-intuitive. Around this intermediate axis, small perturbations grow exponentially and lead to oscillations that can rotate around the other axes.

2.2 Types of Tops

Type	Example	Moment of Inertia Relation
Spherical top	SF_6	$I_a = I_b = I_c$
Linear top	N_2	$I_a = 0, I_b = I_c$
Symmetric top (Oblate top)	C_6H_6	$I_a = I_b < I_c$
Symmetric top (Prolate top)	CH_3I	$I_a < I_b = I_c$
Asymmetric top	C_3H_5ClO	$I_a < I_b < I_c$

Table 2.1: *Types of Molecular Tops*

Different types of tops are identified by how their principal moments of inertia relate to each other. For some highly symmetric molecules, such as sulfur hexafluoride, all the moments are equal. Such molecules are called spherical tops. For a linear top, like nitrogen, almost all of its mass is along one axis. So one component of the momenta of inertia is near zero, and the other two components are equal to each other.

Symmetric tops have two equal moments of inertia; the third moment may be larger or smaller than these two. These two types of symmetric tops are called oblate and prolate, respectively. All of these tops so far are periodic, as in, they return to their initial positions when they start moving.

Just as most everyday objects are asymmetric tops, most polyatomic molecules are asymmetric tops. There is no 3-fold or higher axis of rotational symmetry. Asymmetric tops have three distinct moments of inertia, therefore three fundamental frequencies of the molecule rotating around its axis. When an asymmetric top is rotated, it often does not return to its starting position.

2.3 Laboratory Frame Coordinates

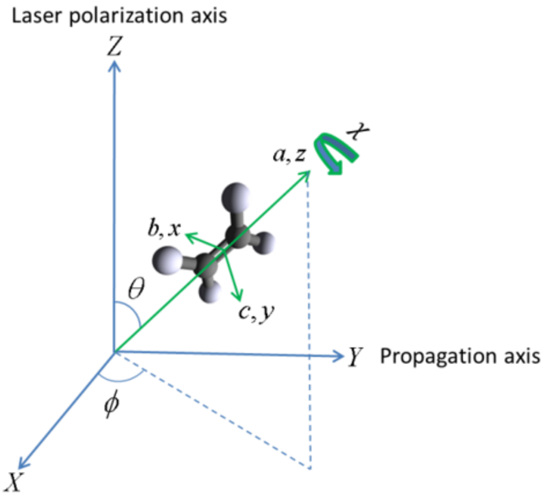

Figure 2.2: *Ethylene molecule in the laboratory frame. The Y and Z axes are defined by the laser propagation direction and polarization, respectively. The axes a, b, and c refer to the axes of the molecular frame in Fig 2.1, and can be written in a convention of z, x, and y. The Euler angles θ, ϕ, and χ are used to describe the orientation of the molecule. This image is from Makhija's thesis*[1]

Solely defining the molecular frame is not enough. The molecule always exists in a space defined by its environment with which often interacts in an orientation-dependent manner. For the experiments considered in this thesis, the laboratory frame is defined using the direction of the laser polarization (Z axis) and the laser's propagation (Y axis). In this new laboratory frame, new angular coordinates described by Euler angles (θ, ϕ, and χ) will be used to describe the orientation of the molecule. θ is the polar angle between the laser polarization Z axis and the molecular z axis. ϕ is the azimuthal angle of the molecular frame z axis about the laboratory frame Z axis. χ is the molecule's rotation along its own molecular axis z.

If a linearly polarized laser is being used, there is cylindrical symmetry in the lab frame. With cylindrical symmetry about the Z axis, the ϕ angles will be irrelevant since all values of ϕ will be equivalent. In this case, only two angles θ and χ are needed to describe the orientation of the molecule.

If the molecule is linear, then the rotation about χ is also physically irrelevant since all χ values are equivalent. The angle dependence of how this linear molecule moves will only depend on the angle θ between the laser polarization axis Z and the molecular axis z.

Now that the laser is used to define the lab frame, an electric field is added to the system, and therefore, a potential is added to the Hamiltonian

$$\begin{aligned} H = \frac{J^2}{2I} &+ V \\ V &= -\overrightarrow{p} \cdot \overrightarrow{E} \\ &= -\alpha \overrightarrow{E} \cdot \overrightarrow{E} \\ &= \sum_{ij} \alpha_{ij} E_i E_j \end{aligned} \tag{2.2}$$

where $\overrightarrow{p}$ is the induced dipole moment of the molecule, and α is the polarizability tensor. When the molecule is subject to the electric field of the laser, the charges in the molecule reorganize, and a dipole moment is induced. The same electric field exerts a torque on the induced dipole that kicks the molecule towards alignment along the polarization of the laser. This dipole moment is proportional to the polarizability. The potential is proportional to the square of the electric field. This quadratic dependence ensures that the interaction survives cycle-averaging over the oscillating electric field.

The potential can be simplified to the equation Eq 2.3 if the molecule is linear or a symmetric top. The polarizability components here are parallel and perpendicular to the molecular axis. Since the laser adds cylindrical symmetry to the electric field, there is no dependence of ϕ at all; a linearly polarized laser cannot induce rotation about the polarization (the Z axis).

For linear and symmetric top molecules, the polarizability tensor has one principal component along the symmetry axis and two equal components perpendicular to it. Therefore, the potential does not depend on the angle χ and the interaction cannot induce rotation around the molecular z axis either. This potential is, therefore, a function only of θ.

$$V \propto -E^2 \cos^2\theta(\alpha_{\parallel} - \alpha_{\perp}) \tag{2.3}$$

For an asymmetric top molecule, the potential is much more complex, as shown in Eq 2.4. Here, α is a tensor written in spherical components rather than Cartesian.

The cylindrical symmetry around the laser polarization remains - the laser still cannot induce rotation around the polarization axis - so the potential does not depend on ϕ. But there is no symmetry around the molecular frame z axis, so the potential depends on the angle χ and the laser can drive rotations around the molecular frame z axis.

$$V \propto -E^2[(\alpha_0^2(\frac{3}{2}\cos^2\theta) + (\alpha_2^2(\sqrt{\frac{3}{2}} sin^2\theta \cos(2\chi))] \tag{2.4}$$

Eq 2.5 shows what the wavepacket looks like of a linear molecule after the interaction with the pump pulse. Where $|JM\rangle$ is the superposition of a particular total angular momentum and the J_a component of angular momentum state. The rotational eigenvalue for this state is $E_J = BJ(J+1)$, where B is proportional to the fundamental frequencies of rotation around the principal b axis from Eq 2.1. J is the total angular momentum quantum number, and M is the azimuthal quantum number. Because the eigenvalues of the field-free Hamiltonian are integer multiples of a constant, the wave function can be written as a Fourier series, shown in Eq 2.5. Therefore, this wavefunction is periodic for linear and symmetric tops.

$$\psi(t) = \sum_J C_{J,M}(0)\,|J,M\rangle\, exp[\frac{-iE_J t}{\hbar}] \tag{2.5}$$

2.4 Identifying Orientation

Linear and symmetric top molecules will have integer multiples of their fundamental frequencies and will have periodic alignments with the polarization of the electric field. Asymmetric tops have different momenta of inertia and will have multiple frequencies involved. These frequencies are not commensurate; therefore, these molecules will not have periodic alignment with the electric field of the laser pulse.

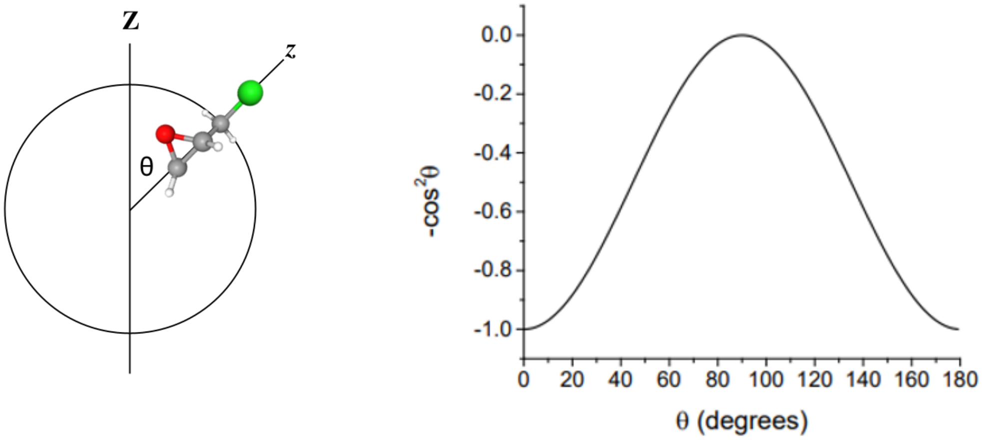

Figure 2.3: *The average* $\cos^2\theta$ *measures the alignment of the molecular* z *axis with the polarization of the laser pulse* Z*. The potential energy is proportional to* $-cos^2\theta$ *(shown on the right).*

Referring to Fig 2.3, the angle θ measures the alignment of the molecular z axis with the laser polarization Z axis. We use the average of $\cos^2\theta$ to measure this alignment, as $\theta = 0°$ and 180° would both align the two axes. The pump pulse initiates rotation of the molecules towards these angles. The molecule gets kicked in the appropriate direction and lines up a time later, after the pulse has gone. For molecules that are not aligned and are randomly orientated, $\langle\cos^2\theta\rangle = 1/3$. As the alignment improves, $\langle\cos^2\theta\rangle$ approaches 1. If the molecule is completely anti-aligned, $\langle\cos^2\theta\rangle = 0$.

Fig 2.4 is from a previous JRML experiment[12] studying rotational dynamics of a linear molecule. Shown on the bottom plot of Fig 2.4 is the trace of $\cos^2\theta$ for N_2. It has a pattern of repeating its alignment to the polarization almost every 5 ps; however, it arrives from different orientations every other time. The top plot shows a signal from degenerate four-

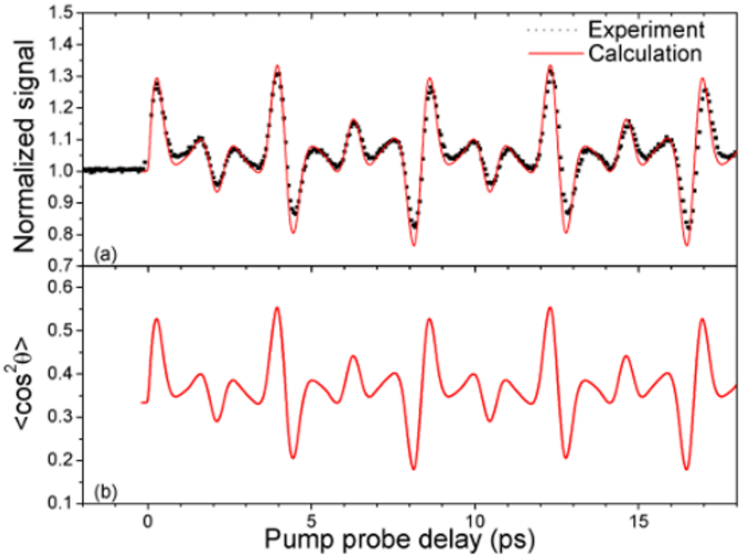

Figure 2.4: *Revivals of N_2 from Ren's thesis*[12]*. The top plot shows the yield of N_2 as the time delay between the pump and the probe pulse increases. Shown on the bottom plot is the* $\cos^2\theta$ *or the alignment of N_2 with the polarization of the laser as the delay increases. There is a pattern to when the molecule is aligned with the laser's polarization, there is more signal yield of N_2.*

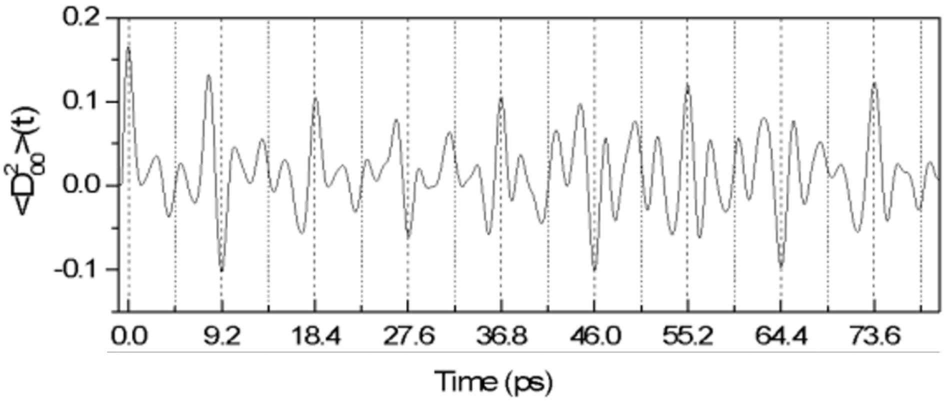

Figure 2.5: *Revivals of C_2H_4 shown with Wigner function $D^2_{0,0}(t)$ from Makhija's thesis*[1]*. Periodic patterns of alignment diminish after 40 ps.*

wave mixing (DFWM); an experimental method to determine the degree of alignment of the molecules.

Fig 2.5 is from another JRML experiment[1] studying rotational dynamics of the asymmetric molecule, ethylene. It is plotted as a Wigner function $D^2_{0,0}(t)$ as the Wigner functions can be used to represent any angular function. For instance, $\cos^2\theta = \frac{1}{3} + \frac{2}{3}D^2_{0,0}$. The Wigner function is linearly related to $\cos^2\theta$.

Wigner functions $D^J_{K,M}(t)$ are eigenstates of the Hamiltonian for a symmetric top, having J, K, and M eigenvalues conserved. In a laser pulse, when there is no dependence on ϕ ($M = 0$), Wigner functions become spherical harmonics. $D^2_{0,0}$ can be written in spherical harmonics Y^2_0.

It is shown in Fig 2.5 that at times 0 ps, around 8 ps, and 18.4 ps, there is more alignment between the molecule and the polarization of the laser. At later times, the dynamics look increasingly non-periodic. For an asymmetric molecule, its moment of inertia has three different frequencies, and the potential is driving the molecule in three dimensions; therefore, the rotational dynamics are non-periodic and complicated.

2.5 Strong Field Dissociative Ionization

The experiment in this thesis is a pump-probe experiment, where a pump pulse initializes the rotation of our molecule. At a later time, a short and intense probe pulse quickly removes an electron, thus making our molecule unstable, and exploding it into fragments of ions. By measuring the position and time that these ions land on a detector, the molecule's orientation can be found at a specific time. The molecule's angular distribution can be found by solving the molecule's Schrodinger equation and calculating its wavefunction, which is set by the pump. Shown in Eq 2.6, $\psi(\theta,\chi,t)$ is the wavepacket of the molecule.

$$\begin{aligned} \rho(\theta,\chi,t) &= |\psi(\theta,\chi,t)|^2 \\ S_{ion}(t) &= \int \rho(\theta,\chi,t) f_{ion}(\theta,\chi,t) sin\theta d\chi d\theta \end{aligned} \tag{2.6}$$

The probability of the molecule producing a particular ion at this position is represented by the function $f_{ion}(\theta,\chi,t)$, which is set by the probe. The convolution of these two functions will result in the signal yield $S_{ion}(t)$ of one particular ion. This is a theoretical way of finding the ion yield. Chapter 3 discusses the experimental way we found these ion yields.

Chapter 3

Experimental Setup

This chapter first describes the optical layout for pump-probe experiments and VMI apparatus. Then it will discuss how we handle data acquisition using the Timepix3, and how our methods were improved over time.

3.1 Experimental Apparatus

3.1.1 Laser

The James R. Macdonald Laboratory (JRML) at Kansas State University (K-State) uses a Coherent Legend Elite Duo Ti:Sapphire laser system (dubbed ”FLAME”) to produce the femtosecond pulses for this experiment. It produces linearly polarized pulses with a central wavelength of 810 nm and a bandwidth of about 50 nm. Pulses from this laser are split into two with a 50%-reflection beam-splitter, having the transmitted beam become the pump pulses and the reflected beam become the probe pulses. A 20-cm-focal-length concave mirror in the vacuum chamber focuses the pulses to the interaction region with the target molecules. A simplified schematic diagram of the experimental setup is shown in Fig 3.1.

The pulse durations were measured using Frequency-Resolved Optical Gating (FROG)[13], shown in Fig 3.2, before the beams enter the interaction chamber. The pump pulse duration is stretched by an SF11 glass plate placed in its optical path which it transmits through.

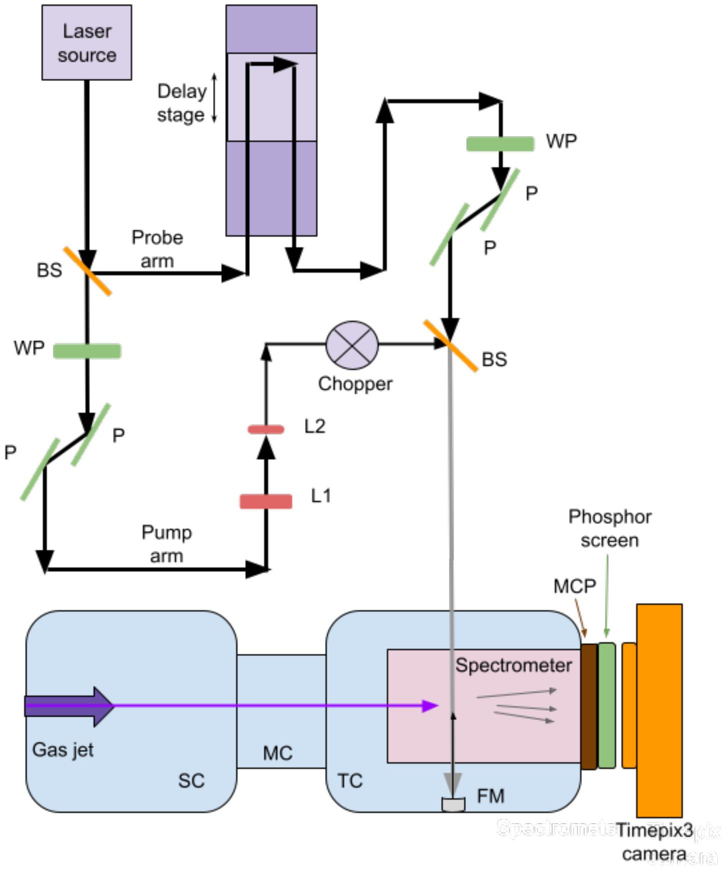

Figure 3.1: *Schematic of experimental setup. The laser passes a beam splitter (BS) that separates the pump arm from the probe arm. Both arms have a set of waveplates (WP) and polarizers (P) to control power. The probe arm has a delay stage to vary the time the probe pulse enters the target chamber after the pump pulse. The pump arm passes through a telescope consisting of a 300 mm lens (L1) and a 200 mm lens (L2), and a chopper that blocks a fraction of the pulses. The source chamber (SC) holds the Even-Lavie valve that generates the gas jet. The middle chamber (MC) maintains the large pressure difference between the source and target chambers. The target chamber (TC) holds the spectrometer. Once both laser arms enter the TC, they reflect off a 20 cm focusing mirror (FM) that focuses the pulses into the interaction region with the molecular gas beam. The ionic fragments will flow towards the MCP detector and the phosphor screen. The Timepix3 camera collects information from the flashes that the phosphor screen creates. Details about the valve and the spectrometer are provided in sections 3.1.2 and 3.1.4, respectively.*

The focal spot size of the pump beam is approximately twice as large as the size of the probe beam due to the telescope in the pump arm. A smaller probe spot size means we only detect molecules from near the peak of the pump pulse intensity profile. This is where the molecules experience the most torque and have more alignment.

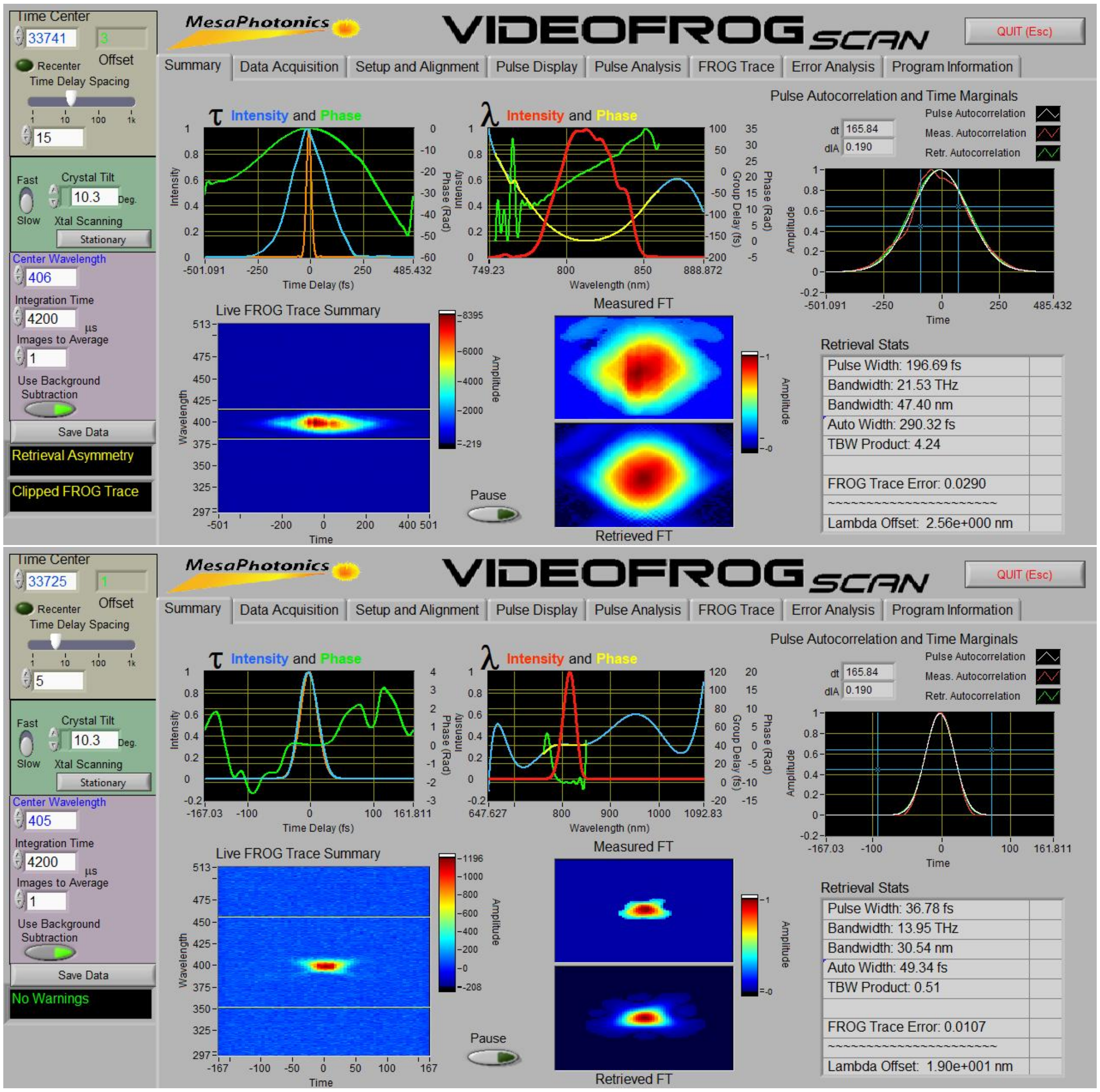

Top (pump):

Time Center 33741, Offset 3
Time Delay Spacing 15
Crystal Tilt 10.3 Deg.
Xtal Scanning: Stationary
Center Wavelength 406
Integration Time 4200 µs
Images to Average 1
Use Background Subtraction
Retrieval Asymmetry
Clipped FROG Trace
dt 165.84
dIA 0.190

Retrieval Stats
Pulse Width: 196.69 fs
Bandwidth: 21.53 THz
Bandwidth: 47.40 nm
Auto Width: 290.32 fs
TBW Product: 4.24
FROG Trace Error: 0.0290
~~~~~~~~~~~~~~~~~~~~~~~~
Lambda Offset: 2.56e+000 nm

Bottom (probe):

Time Center 33725, Offset 1
Time Delay Spacing 5
Crystal Tilt 10.3 Deg.
Xtal Scanning: Stationary
Center Wavelength 405
Integration Time 4200 µs
Images to Average 1
Use Background Subtraction
No Warnings
dt 165.84
dIA 0.190

Retrieval Stats
Pulse Width: 36.78 fs
Bandwidth: 13.95 THz
Bandwidth: 30.54 nm
Auto Width: 49.34 fs
TBW Product: 0.51
FROG Trace Error: 0.0107
~~~~~~~~~~~~~~~~~~~~~~~~
Lambda Offset: 1.90e+001 nm

Figure 3.2: *Second harmonic FROG traces of the pump (top) and the probe (bottom).*

The pump pulse passes through a chopper in a way that blocks four pulses and allows the next four to reach the chamber. This chopper reduces the frequency of the pump pulse to 1500 Hz. We collected data for several pump and probe powers, but this thesis will only discuss one set of powers. This pump pulse enters the chamber with a power of 60 mW, pulse duration of about 200 fs, and estimated intensity of 7.6e12 W/cm^2. The intensities are found by integrating over the full distribution of each beam (which is a product of three

Gaussian functions in terms of X, Y, and time), and dividing the energy per pulse by this volume.

The probe pulse goes through a delay stage to vary the time the target molecule has to rotate before the probe pulse ionizes it. With epichlorohydrin having an ionization energy of 10.4 eV, the probe pulse has enough intensity to induce Coulomb explosion. The probe enters the chamber at a frequency of 3 kHz, power of 130 mW, pulse duration of 37 fs, and estimated intensity of 1.5e14 W/cm^2. The translation stage (Newport IMS300PP) is controlled using a computer and LabVIEW program.

Half-wave plates and sets of flat polarizers are used in both beams to independently control the power. The beams are recombined and pass another beamsplitter, and enter the vacuum chamber, where they both back reflect off the focusing mirror and interact with our target sample.

3.1.2 Supersonic Molecular Beam

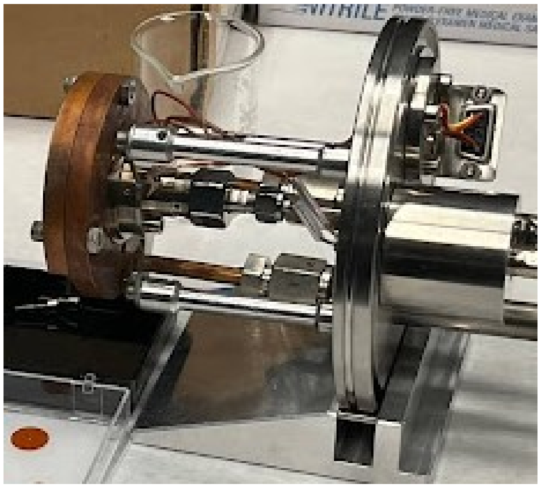

Figure 3.3: *Even-Lavie valve outside of the source chamber.*

We strive for our gas molecules to be as close to 0 K as possible. The Even-Lavie valve creates a supersonic gas jet where molecular vibrations and rotations are cooled to temperatures of a few Kelvin. At these temperatures, the internal degrees of freedom are limited, and we can focus on only the rotational states. Through supersonic expansion, molecules are also produced as a gas phase without condensation[14]. A more in-depth discussion and applications of cold gas-phase molecules can be found in Levy[14] and Carr[15]. Another advantage for a molecule like epichlorohydrin is that at a few Kelvin, we expect the lowest energy conformer. For both R and S isomers, these conformers differ in the rotation of the CH_2Cl and the rest of the molecule[16]. Knowing that the R and S isomers have three conformers each, we can cool the temperature to reduce the three possibilities of each isomer to just one.

Epichlorohydrin is a liquid at room temperature. A glass filter paper is soaked in the liquid and placed in a sample holder within the Even-Lavie valve. Helium at 1000 psi is used as a carrier gas for the sample molecules. As the mixture of helium and the sample expands from the nozzle of the Even-Lavie valve, the molecules are adiabatically cooled to a few Kelvin.

The mix was delivered as a supersonic molecular beam created by expansion through a pulsed Even-Lavie valve[17]. The Even-Lavie valve releases the gas mixture as a pulsed beam at a frequency of 750 Hz and with a pulse duration of 6.6 μs. Although we have not yet determined the rotational temperature of this sample, the typical values are 1-3 K.

From this gas mixture, only epichlorohydrin and its fragments will be ionized, as helium needs a lot of energy to be ionized. Helium requires 24.58 eV and, thus, much higher laser intensities to be ionized compared to epichlorohydrin at an ionization potential of 10.6 eV. Even the fragments produced are much easier to ionize than helium, such as atomic oxygen at 13.61 eV. From our data collected, we do see some helium, but much less than the fragments from the molecules.

3.1.3 Vacuum Chamber

In our schematic in Fig 3.1, we have three chambers kept under a vacuum with turbomolecular pumps to isolate our target molecules and prevent contaminants. The source chamber maintains a pressure of approximately 1e-5 Torr while the gas jet in this chamber runs at 750 Hz. The source chamber is separated by the middle differential pumping chamber, which is then separated from the target chamber. These separations are made using skimmers of 3 mm in diameter and a gate valve between the middle and source chambers. The gate valve is open while the experiment is running, but it can be closed if the molecular beam source needs to be serviced. The middle chamber is kept at a pressure of 1e-8 Torr and the target chamber at approximately 1e-9 Torr with the gas beam running. All pressures were measured using nude Bayard-Alpert ionization gauges.

3.1.4 Velocity Map Imaging Spectrometer

Figure 3.4: *VMI spectrometer outside of the chamber*

The gas sample enters the target chamber, gets rotationally excited by the pump pulse and is ionized by the probe pulse, then its fragments continue traveling down the spectrometer towards the detector. A technique called Velocity Map Imaging (VMI) is used to identify charged particles with equal transverse velocity components to the same point on the detector[18]. The spectrometer has three plates creating an imaging lens. These plates consist of the repeller, extractor, and ground plates. These plates create an electrostatic lens that focuses charged particles with equal velocity perpendicular to the plane of the detector to the same location on the detector. The repeller (at 1500 V) and the extractor (at 1200 V) are connected with high voltage power supplies outside of the chamber, while the ground plate is connected to the wall of the chamber. Further discussion about the VMI design can be found in Lam's thesis[11]. The entire VMI spectrometer is enclosed in a mu-metal casing to prevent interactions with unwanted magnetic fields.

After passing through the skimmers of the middle chamber, the gas beam enters the target chamber and the VMI spectrometer between its repeller and extractor plates. This is the interaction region, where the molecular beam interacts with the pump and probe laser pulses. The resulting ions are pulled by the nonuniform electric field through the spectrometer towards the detector. The detector comprises two microchannel plates (MCP) in a chevron configuration[19] and a phosphor screen behind it. A single MCP consists of a glass plate with a regular grid of small holes called channels. When a high voltage is applied between the MCP surfaces, each channel acts as an electron multiplier. The initial electron emission is triggered by an incoming particle hitting the front surface of the MCP, followed by a cascade of secondary electron emissions that results in the emission of approximately 10^3 electrons from the back surface. A stack of two MCPs can generate approximately 10^6 electrons for every incoming particle. These electrons are then accelerated towards a phosphor screen, resulting in a short burst of light emission that is visible to the naked eye. The Timepix3 detects these bursts of light from the phosphor, recording both the position and time of the ion impact on the front surface of the MCP. The front surface of the MCP is grounded, the back surface is maintained at 2000 V, and the phosphor is held at 5000 V.

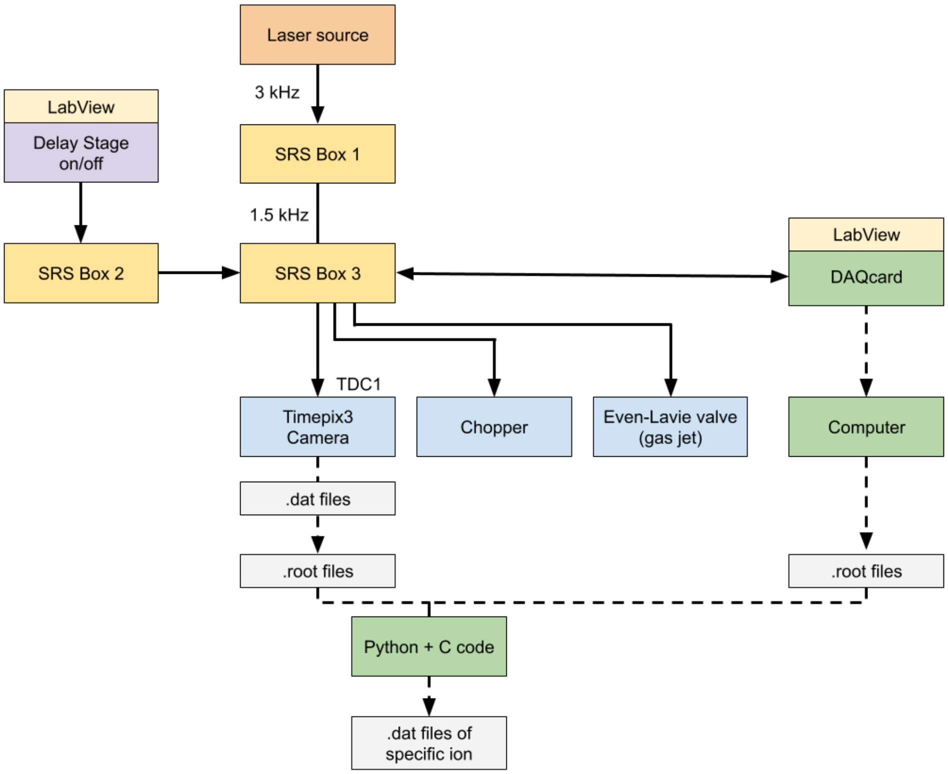

Figure 3.5: *A flowchart showing the stream of electronic connections and data outputs. Solid lines are electronic connections. Dashed lines are digital connections. SRS = Stanford Research Systems DG535 digital delay generator. DAQ card = Data Acquisition Card PCIe6353. The laser's initial 3 kHz rep rate halves through SRS Box 1. SRS Box 2 collects the timing of the delay stage movements. SRS Box 3 triggers the Timepix3 camera, chopper, and Even-Lavie valve at their respective frequencies. SRS Box 3 also sends this timing synchronization information to the computer, where it makes .root files. The Timepix3 creates .dat files, which can be made into .root files. These two types of .root files can be combined in Python and C scripts to make .dat files of all the timing and spatial information of each event for a specific ion.*

3.2 Data Acquisition

Fig 3.5 shows the connections of electronics to run this experiment and collect data[20]. The Timepix3 camera has timing information about the laser pulses and the delay stage movements connected via a time-to-digital converter (TDC). The Timepix3 collects this timing information at 1500 Hz and records the detector's pixel information. It creates .dat files that hold raw data of clusters of pixels representing each ion. This data is then centroided and compressed using ROOT, which is a data analysis package from the European Organization for Nuclear Research (CERN). The output is a .root file, in which data is stored in trees in a hierarchical format. Every ion typically triggers several pixels, which form a cluster. Each cluster is saved as a branch and contains information about TOA, TOT, and spatial positions in its leaves. A centroiding algorithm determines which pixel best represents the position and time of the ion's impact. This results in a more precise determination of the actual hit information for each ion.

Independently, the delay box is also used to control moving equipment as the experiment runs, such as the Even-Lavie valve and the chopper. The probe runs at 3000 Hz, the chopper at 375 Hz, and the gas jet at 750 Hz. The Timepix3 camera is triggered at 1500 Hz, so it is missing every other laser pulse. This is because the fastest the gas jet can run is 1000 Hz. Therefore, the timings of the Timepix3 camera, gas jet, and chopper are some fractions of the 3000 Hz laser pulses. These timings are set by a delay box, and the digital signal is recorded by a National Instruments multifunction DAQ card (NI PCIe 6353) operated using a LabVIEW program. This program records timing information in a TDMS (Technical Data Management Streaming, a National Instruments file format) file, which is later converted to a .root file.

These two .root files are combined using Python and C scripts to create a large tree. This tree has branches representing every event the detector saw, and the leaves are the characteristics of that shot. Each branch would have TOT, TOA, X, Y, if the pump was on, if the gas jet was on, and information about the delay scan. The Time of Flight (TOF) can be found for all ions. Choosing a specific interval on this TOF can isolate one particular ion, and more informative plots can be made. Results shown in Chapter 4 are made by gating on specific intervals of TOF.

3.2.1 Stanford's Varian Physics Laboratory

The Timepix3 camera is a piece of equipment that is not commonly used within the James R Macdonald Laboratory (JRML). I visited Dr. Phil Bucksbaum's Varian Physics

Laboratory at Stanford University to observe how they use their Timepix3 camera with their pump-probe experiments. Rather than having a pulsed gas jet, the Varian Physics Laboratory has a continuous gas flow through a leak valve, and they did not implement a chopper or other equipment that blocks pulses. Unlike our multi-parameter scans with a pulsed gas jet, chopper, and moving stage, they just had single-parameter scans with only their delay stage moving.

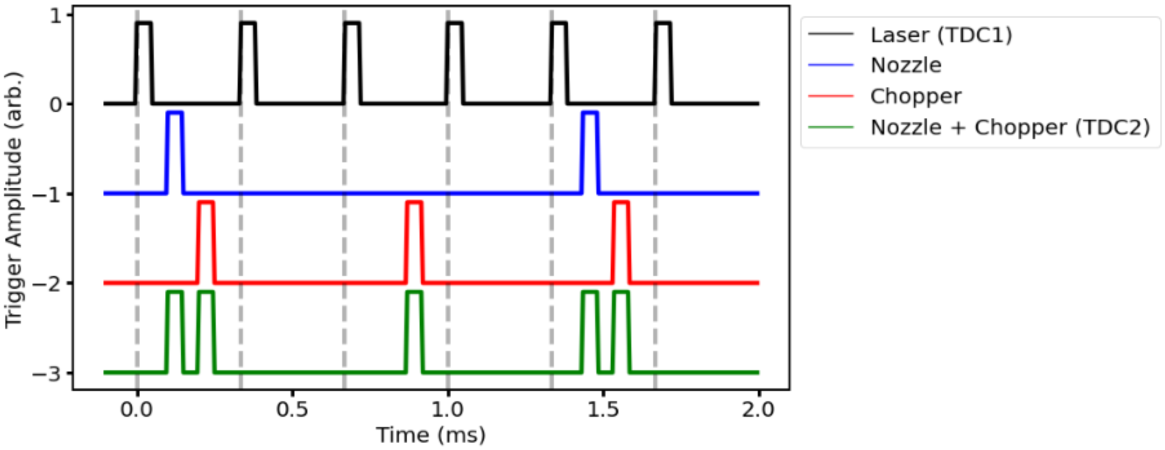

Figure 3.6: *Proposed multi-parameter trigger timings from collaboration with Varian Physics Lab. The black line is our 3 kHz laser input into TDC1. The blue line is the timing of our gas jet at 750 Hz. The red line is the chopper timing at 1500 Hz. The green line is the combination of the nozzle and chopper timings into TDC2. From the TDC1 and TDC2, the Timepix3 camera can synchronize all the timing information of external equipment into one stream.*

We tested a different way of acquiring data for multi-parameter runs. The second time-digital-converter (TDC2) port can be used to encode all external timing information, such as from the gas jet and the chopper. For K-State's experiment, each of these pieces of equipment is tied to run at one-fourth and half the rep rate of the laser, respectively. TDC2 can accept a trigger signal that encodes the status of these moving parts and can write out this information into the Timepix3 to read in directly. The trigger timings can be seen in Fig 3.6. The input from the laser trigger would enter TDC1 like previously, and input the summed triggers of the nozzle and chopper into TDC2.

By having these TDC inputs directly into the Timepix3 camera, we can streamline our output from the Timepix3 camera. The Timepix3 can produce .tpx3 files that have both Timepix3 information (ToA, ToT, X, Y) and external conditions information (gas on/off, pump on/off). From these .tpx3 files, we can continue using Python and C conversion codes that produce specific information that we want. This reduces K-State's need for .root files and offers a way for Stanford to perform experiments with multiple parameters. During this visit, we tested this implementation of using TDC2 at Stanford. We ended up using a similar scheme in K-State.

A more significant thing we learned from Stanford is how they analyze their data. The results in this thesis were created using software that is modeled on their analysis code they shared. This involves a hierarchical .hdf5 file that holds all the information that is collected by the Timepix3 camera. This .hdf5 file has timing information of when the gas jet is on/off, when the chopper is on/off, the TOA, TOT, x, and y of every shot collected, similar to a .root file. This large dataset can be read into and analyzed using just Python. This simplified and sped up our analysis process.

Chapter 4

Results and Discussion

4.1 Sorting Data According to Experiment Status

Every ionic fragment, or event, is detected by the MCP, and this detection is shown as light flashes by the phosphor. These flashes of light trigger a cluster of pixels on the Timepix3 camera. Since the Timepix3 camera knows when each external parameter was on (i.e, the gas beam, the chopper), these events can be categorized into four statuses where a combination of these external parameters was present: gas+pump+probe, pump+probe, gas+probe, or just probe. Fig 4.1 confirms that the timings of the external parameters are fine and that the four statuses are cleanly separated.

4.2 Identifying Ions

Plotting the TOF shows peaks of ionic fragments shown in Fig 4.2. These peaks can be identified by using the linear relationship between the TOF and the square root of the mass-over-charge ratios of each ion: $sqrt(m/q) = a(TOF)+b$. The slope, a, and the y-intercept, b, can be found by knowing the TOF and mass-over-charge of two ions. He^{+} and $C_3H_5ClO^{2+}$ was chosen for our data. The slope constant was 7.47e-6 and 7.40e-6 for the S and R isomers, respectively. The y-intercept was 0.475 and 0.452 for the S and R isomers, respectively. Ions

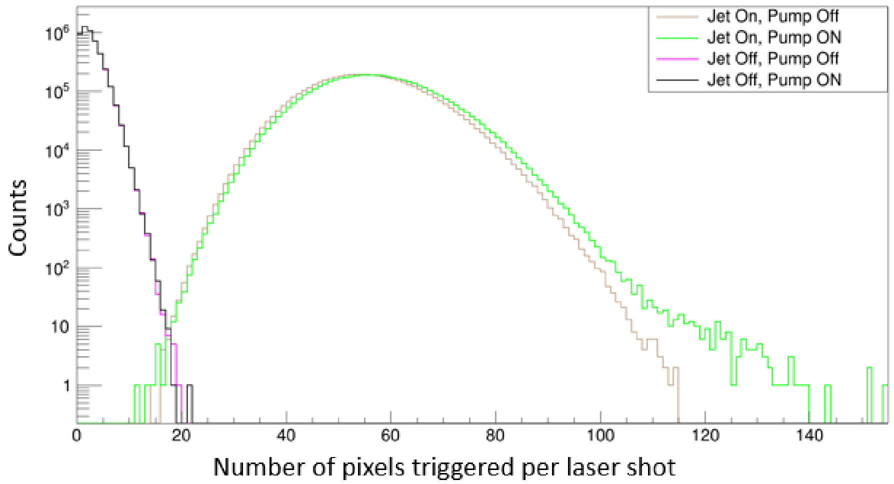

Figure 4.1: *When there is no gas jet (black and pink lines), the Timepix3 camera typically observes few pixels (fewer ions) triggered in a laser shot. When there is a gas jet (brown and green lines), there are many instances where a higher number of pixels are being triggered in a laser shot (around 60 pixels per shot).*

with smaller mass-over-charge ratios would fall earlier in the TOF, as these fragments have more velocity (to compensate for less mass but the same kinetic energy as other ions) and travel faster to the detector.

Fig 4.3 shows the TOT vs X position of the ion impact on the detector. Some of the TOF peaks appear as ellipses in this plot, which is an indication that the corresponding ions are produced with significant kinetic energy from their breakup. If the energetic ions are emitted towards or away from the detector, their TOF will be shorter or longer than ions that have no kinetic energy or that are emitted parallel to the detector's surface.

Many of the ions identified in these plots are singly charged. They may still be from double ionization if the partner ion is also charged. We also see counts of doubly charged ions, such as C^{2+} and $C_3H_5ClO^{2+}$. With epichlorohydrin having an ionization energy of 10.6 eV, and from previous experiments at K-State[21], we know that this molecule is known to fragment to many different fragments even if it is just singly ionized.

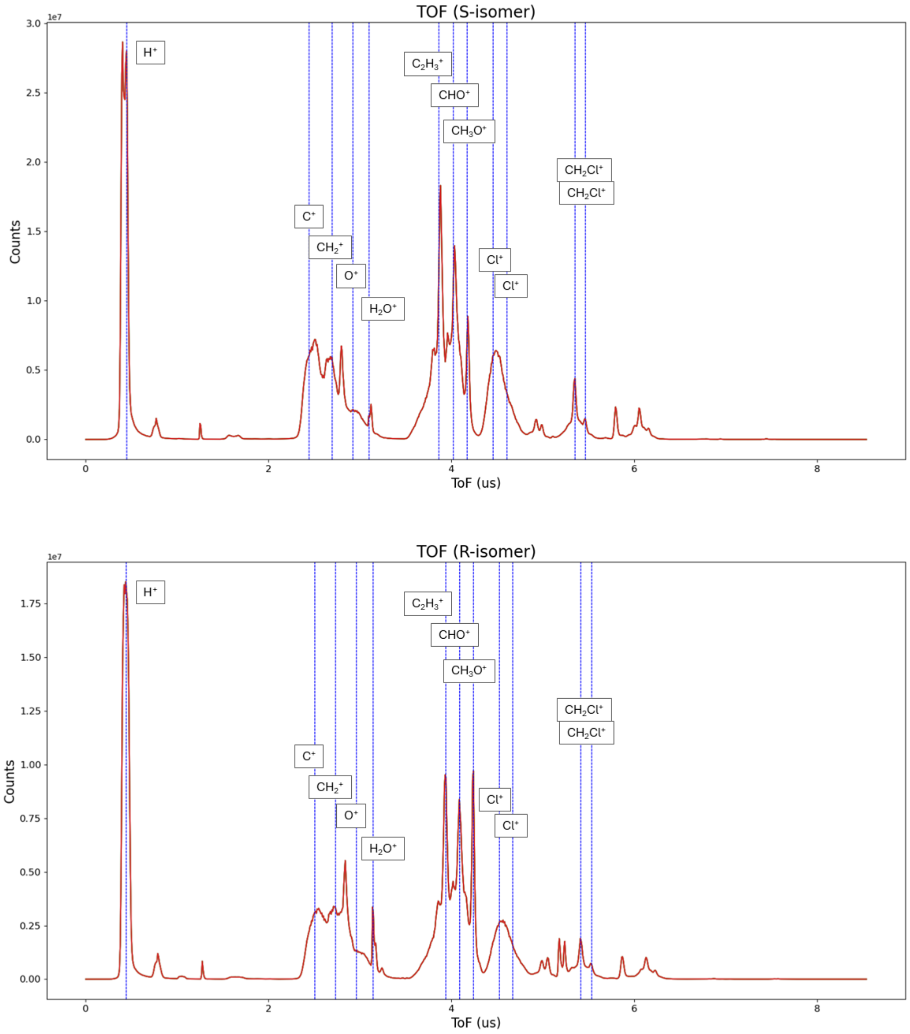

Figure 4.2: *TOF of S-isomer (top) and R-isomer (bottom) epichlorohydrin (C_3H_5ClO) for shots with gas, pump, and probe pulses occurring. Dashed lines label some ions. Some ions with chlorine are labeled twice to include the 35 and 37 isotopes.*

4.3 Signal Yield of Ions and Alignment

From the pixels that the Timepix3 camera observes, we want to see the signal yield of ions. Experimentally, this can be found using the information from Eq 4.1; where the alignment signal has the gas jet on, pump pulse entering, and probe pulse entering. The isotropic signal has the gas jet on and only the probe pulse. The background terms do not have the gas pulse. Background subtraction must be considered when the gas jet is present (when the target molecule is there). Division of the isotropic signal is important to correct

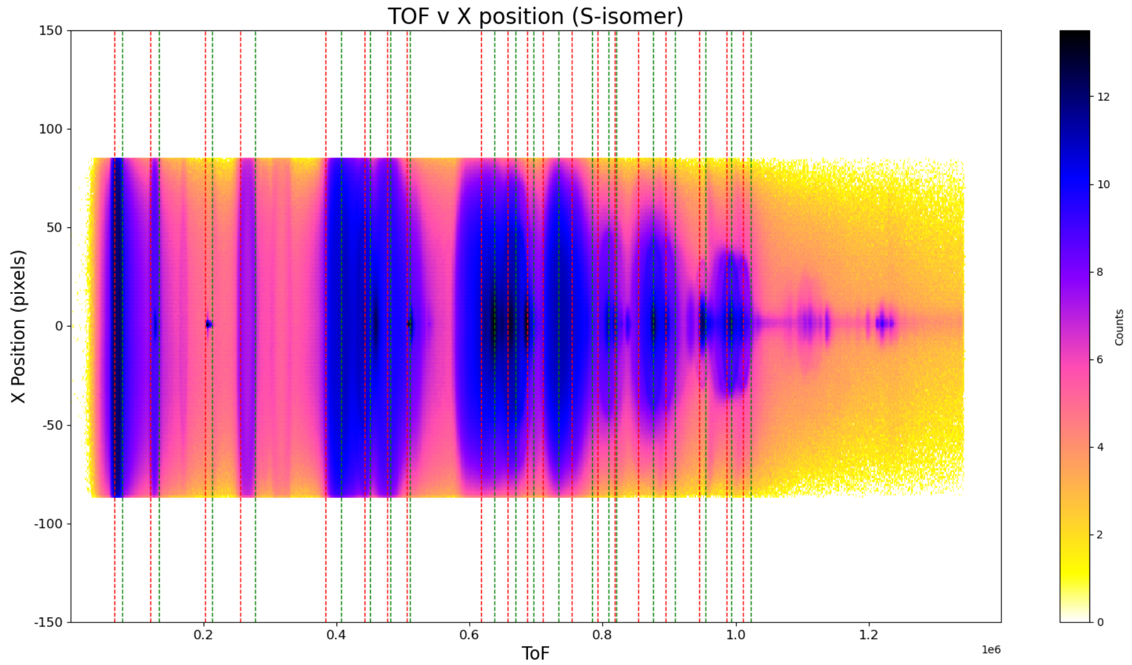

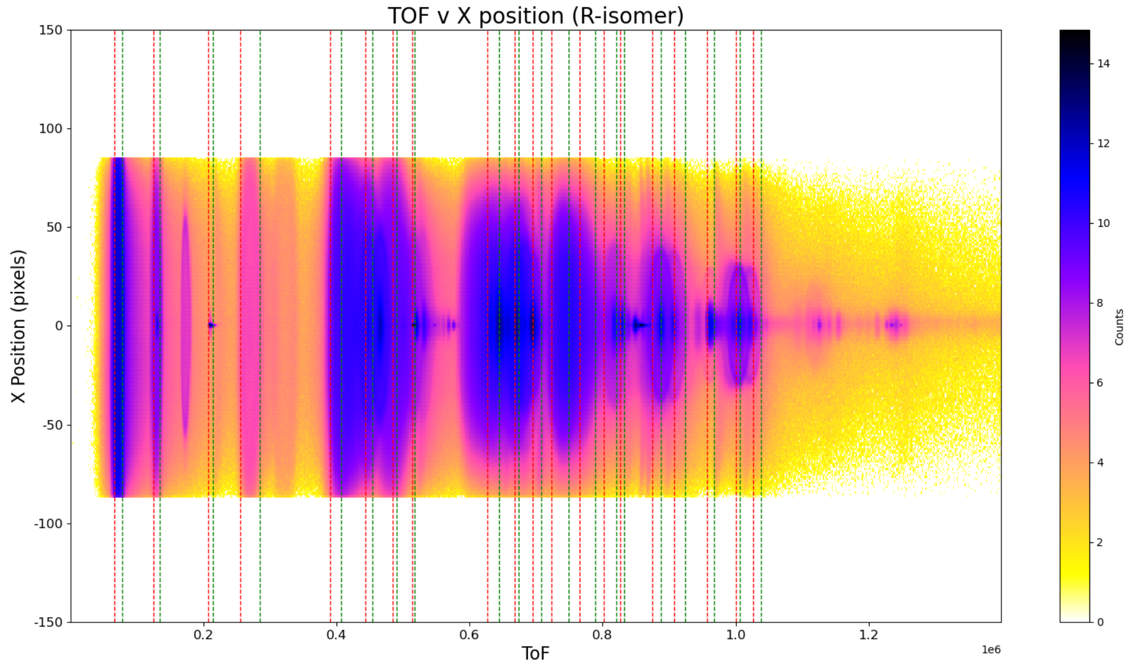

Figure 4.3: *Time of Flights (TOF) versus the X positions of fragments of S-isomer (top) and R-isomer (bottom). The horizontal axis is in units of the Timepix3 clock ticks, where each clock tick equals (25e-9 / 4096) * 1e6 picoseconds. The red dashed lines show where the gates of each ion start and the green dashed line shows where the gates of each ion end. The counts of events in each pixel are in log(e) form for better visibility of each fragment.*

the changes in gas density that occur with the pulsed gas jet.

$$\begin{aligned}\text{Normalized signal yield} &= \frac{\text{(Alignment signal)} - \text{(background with pump and probe)}}{\text{(Isotropic signal)} - \text{(background with just probe)}} \\ &= \frac{\text{(gas+pump+probe)} - \text{(pump+probe)}}{\text{(gas+probe)} - \text{(background with just probe)}}\end{aligned} \tag{4.1}$$

Fig 4.4, 4.5, and 4.6 show the normalized signal yield of various ionic fragments using the Eq 4.1. From these plots, we can identify certain times that the molecule was aligned with the polarization of the laser to produce more of that ion. The very first peak of these plots is the signal when the most polarizable axis of the molecule is aligned with the polarization of the laser.

In our experiments, the delay scans were repeated 25 times. Averaging over these scans takes into account any drifting or changes in the environment (i.e, the temperature or humidity of the room) as the data was being collected. The purple band on these plots is the standard deviation of these 25 scans. The standard error of the mean is $1/\sqrt{25} = 1/5$ of the size of this band (and is not shown in the plots).

In the plot for hydrogen, in Fig 4.4, the molecule aligns itself in a certain way around time 120 ps, produces a large amount of H^+ ions, then immediately rotates in an orientation that produces very few H^+ ions. This alignment act, or revival, reoccurs at certain times. However, the yield at these revivals diminishes in time.

In the figure, there is a significant difference between the two isomers, that being the partial revivals. We can see partial revivals between the larger peaks only in the R isomer. We believe that it is because the intensity of our pump pulse has increased in the days that we collected data.

In Fig 4.5, the 35-isotope of Cl^+ is shown to have a large yield around time 120 ps and immediately drops in yield after. Since chlorine is attached at one end of the epichlorohydrin molecule, one can assume that at this time, the molecule has its polarizability axis line up with the polarization of the laser pulse. Cl^+ is produced preferentially at this particular time, when the two axes are lined up. Similarly, H^+ is produced more when the molecule

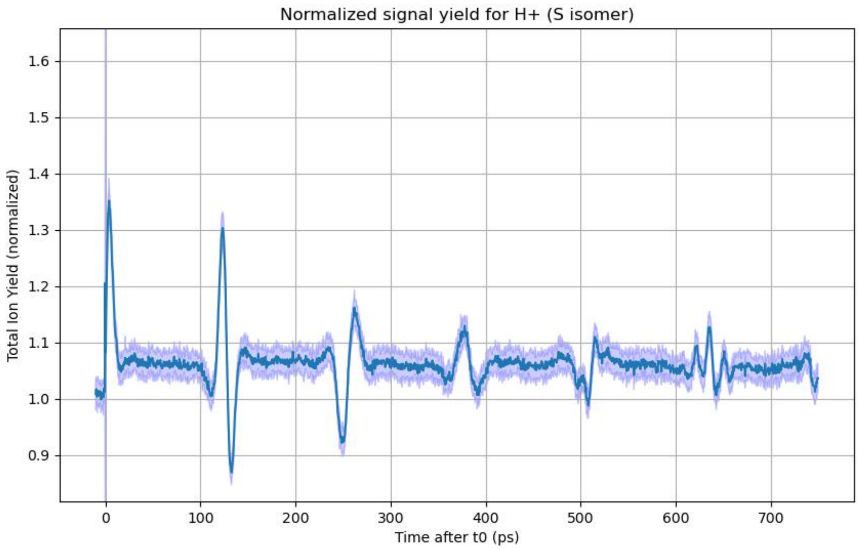

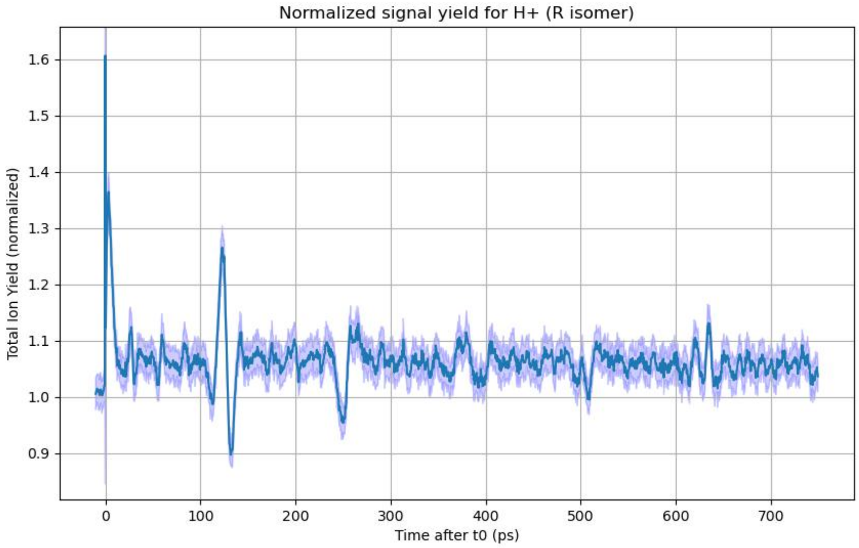

Figure 4.4: *Normalized signal yield of H^+ of S-isomer (top) and R-isomer (bottom). The horizontal axis is the time between the pump and the probe pulses. The purple band is one standard deviation. The signal of H^+ in the R-isomer has visible partial revivals, where there are patterns of rotation in between large revivals (three small, yet clear, peaks between 0 ps and 120 ps). We believe that these partial revivals are shown because of an increase in intensity of our pump pulse for the R isomer.*

is aligned. However, the ionic version of the remaining fragment ($C_3H_5O^+$) would have less yield when there are more Cl^+ ions, which is shown to be true in Fig 4.6. Its peaks are the reversal of the Cl^+ and H^+ peaks.

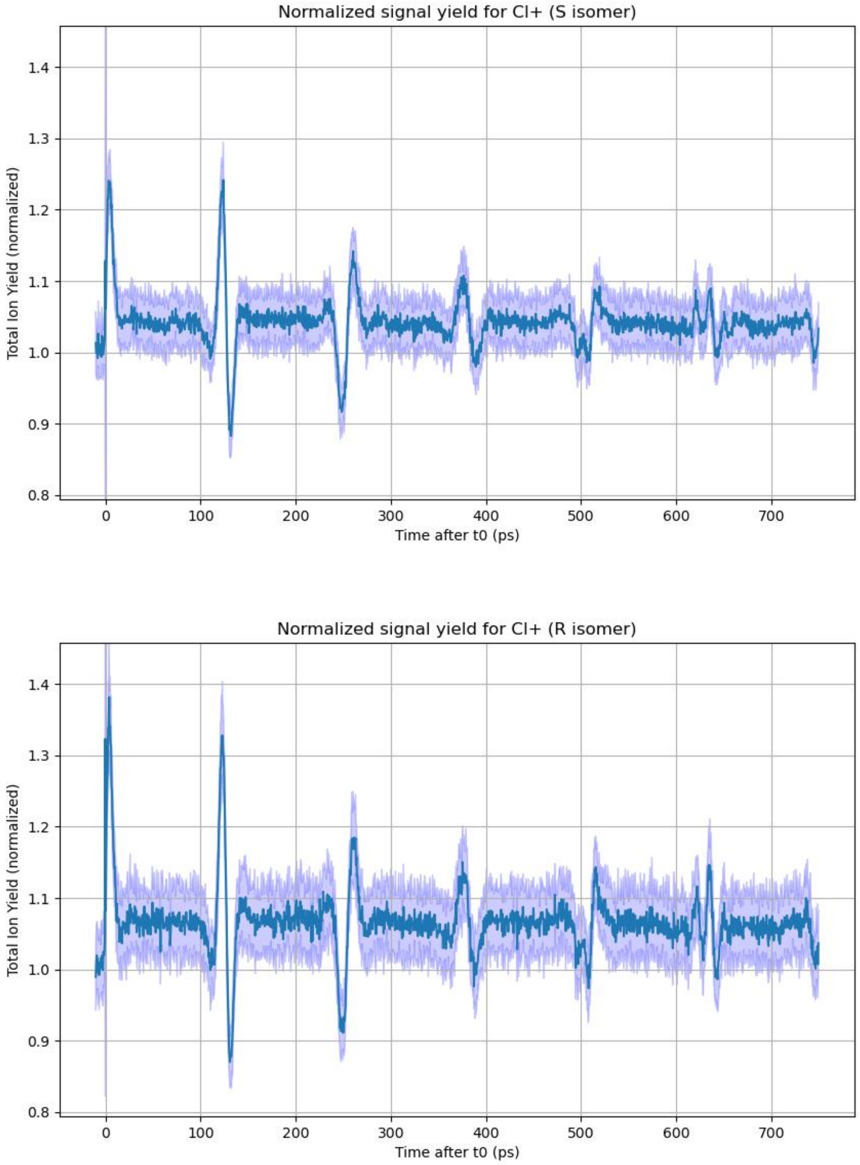

Figure 4.5: *Normalized signal yield of* $^{35}Cl^{+}$ *of S-isomer (top) and R-isomer (bottom. The horizontal axis is the time between the pump and the probe pulses. The purple band is one standard deviation. Around 120 ps, we can infer that the molecule is aligned with the polarization of the laser as more* $^{35}Cl^{+}$ *ions are produced. Immediately after this peak, the yield drops, assuming that the molecule is perpendicularly aligned with the laser's polarization. The revivals of* $^{37}Cl^{+}$ *would arrive at slightly later times, as it has a higher mass.*

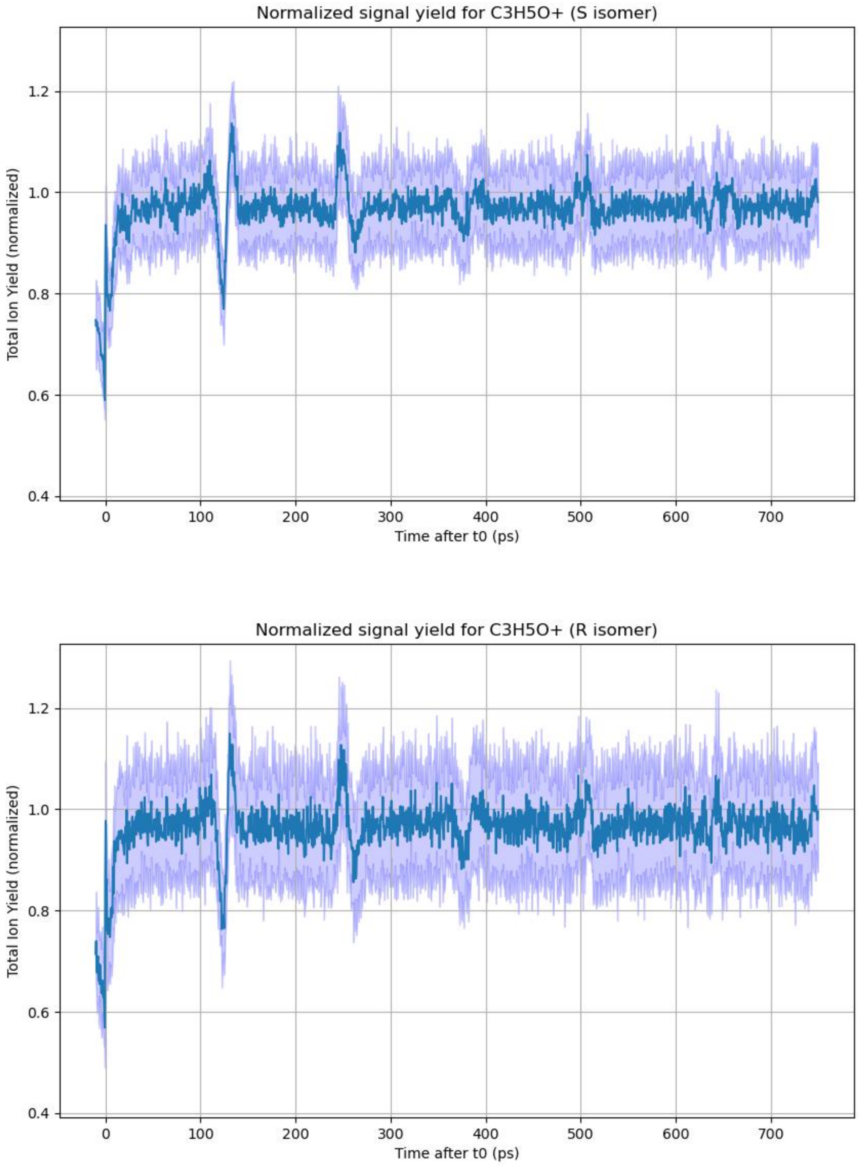

Figure 4.6: *Normalized signal yield of $C_3H_5O^+$ of S-isomer (top) and R-isomer (bottom). The horizontal axis is the time between the pump and the probe pulses. The purple band is one standard deviation. Notice that the revivals are in the opposite direction compared to Cl^+.*

There are three types of conformers of epichlorohydrin, shown in Fig 4.7 and mentioned in Section 3.1.2. Up to this point, the images of epichlorohydrin in this thesis have been of Gauche-II (for easy visualization). Each conformer has different molecular constants. We can identify what type of conformer our gas sample held, or if it contained a combination of conformers, by comparing our experimental time of revivals to the calculated time of arrivals based on the conformers' molecular constants[22, 23].

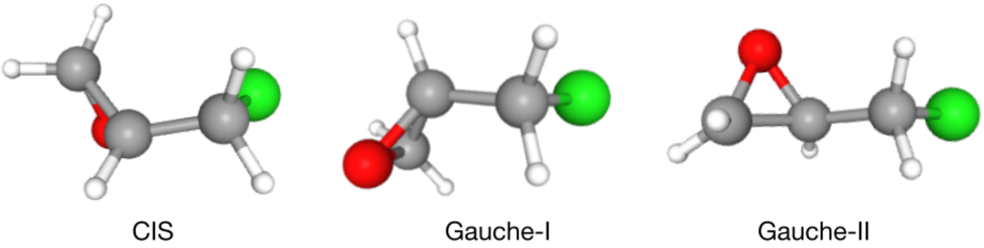

Figure 4.7: *Types of conformers of epichlorohydrin identified by Endo*[23]*. Notice the position of the oxygen with respect to the chlorine. Figures are from PubChem*[10]*.*

Epicholorhydrin can be considered as a prolate-like asymmetric top, as one moment of inertia is much larger than the other two. We have already established that this molecule will have stable rotations, or revivals, around the principal axes a and c. We will call these revivals A-type and C-type revivals. The times of these revivals are at $t \approx n/4A$ and $t \approx n/4C$ respectively, with n being an integer and A and C being the fundamental frequencies. There is also a J-type revival with its time being $t \approx n/2(B+C)$, with B being another fundamental frequency[24].

The molecular constants[23] of each type of conformer can be substituted into these calculations to find the various types of revival times for different conformers. Gauche-I is the conformer for the ground state (when the temperature of the molecule is cold enough). The molecular constants and revival times between Gauche-I and Gauche-II are similar to each other compared to the CIS conformer.

The time between the first peak and the first valley (corresponding to J-type revivals) for our $^{35}Cl^{+}$ data is 128 ps. This matches the calculated time of the first revival for the Gauche-

I type conformer. This confirms that the molecules are primarily the ground conformer in our cold molecular beam.

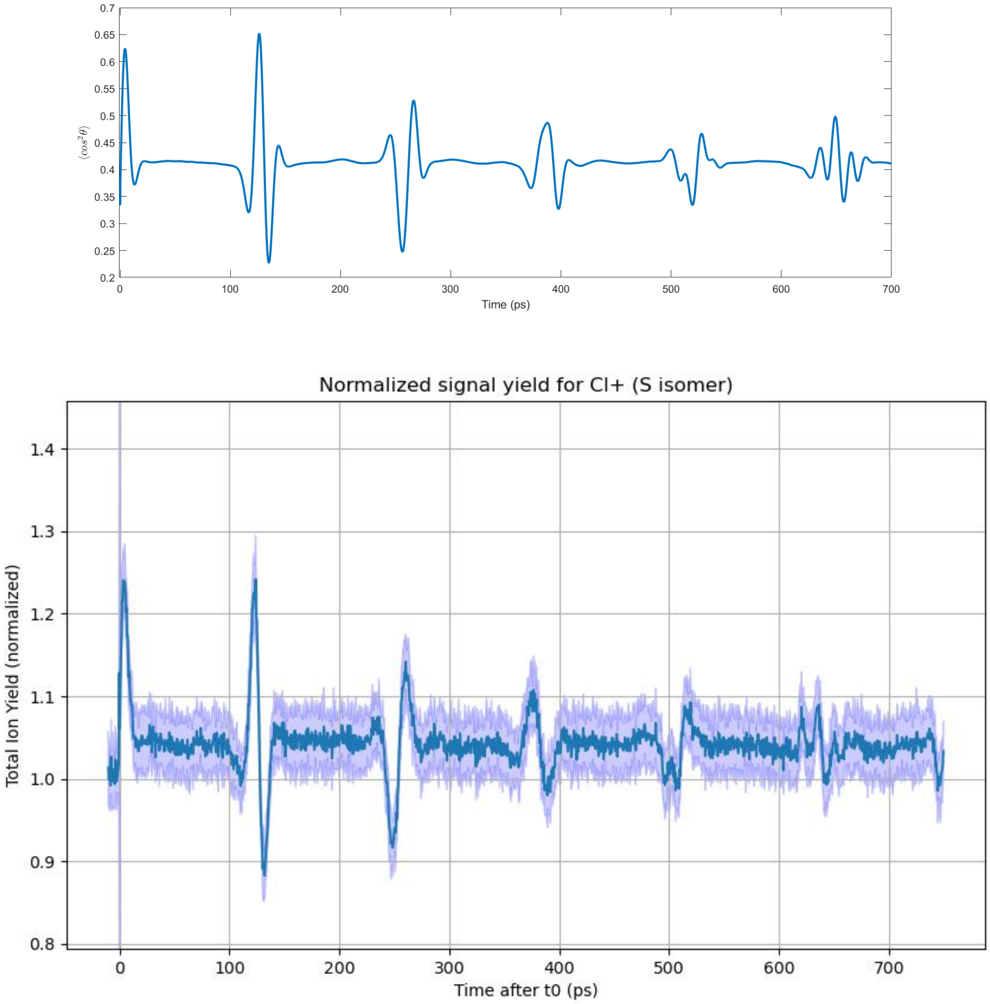

Figure 4.8: *Top: Simulated revivals of epichlorohydrin with a pump intensity of 4e12 W/cm*^{2}*, 100 fs pulse duration, and molecular beam temperature of 1 K. Bottom: Signal yield of* $^{35}Cl^+$ *from our studied S-isomer sample at 7.6e12 W/cm*^{2}*, 200 fs pulse duration, and molecular beam temperature of about 2 K.*

Compared with a simulated calculation of epichlorohydrin's revivals in Fig 4.8, our revivals occur around the same time as the simulated ones. However, ours has two great structures showing motion (the peak and valley) at each revival, while the simulated one has more smaller structures at those times. We can assume that these smaller structures are from the simulation using a lower temperature for the molecular beam. Usually, higher intensities and lower temperatures show more revivals. Our experimental pump intensity is higher, but our temperature is also higher, so our signals do not have such detailed structures.

Since these plots look very similar, we can use our signal yield plots as a proxy to estimate the alignment of our molecule. Our signal yield of $^{35}Cl^{+}$ has the same structure as this simulated epichlorohydrin in the top plot of Fig 4.8. We can use this to estimate our molecule's alignment at the peak of the revival around time 120 ps, which at that plot is $\langle \cos^2 \theta \rangle = 0.6$.

4.4 Momentum Distribution of Ions

By gating the start and end times of the TOF, we can choose specific ionic fragments to observe. The positions of these fragments are proportional to the momentum components in the plane of the detector. Fig 4.9 shows momentum plots of $^{35}Cl^{+}$ at the peak and valley of a revival peak (at 123 ps and 132 ps).

At the peak of the revival, where there are more counts of $^{35}Cl^{+}$ at 123 ps, more of the ions land on two poles on the P_Z axis. This matches our theory that the molecule was aligned with the polarization of the laser at this time (as the polarization of the laser is also the Z direction). At the valley of the revival, where there are fewer counts of Cl^{+} at 132 ps, the momentum distribution of Cl^{+} is more isotropic.

These momentum plots are at the peaks and valleys of the signal yield plots; however, some of these plots show momentum being isotropic. This is because the dissociation is slow, and the fragments forget the molecule's orientation when it was ionized by the time it reaches the detector. For the intensities in this thesis, many of the momentum plots look isotropic despite the fact that there is a large yield of ions. If we want to extract the orientation directly from the momentum distribution, we would need to run the experiment again at a higher probe intensity[8].

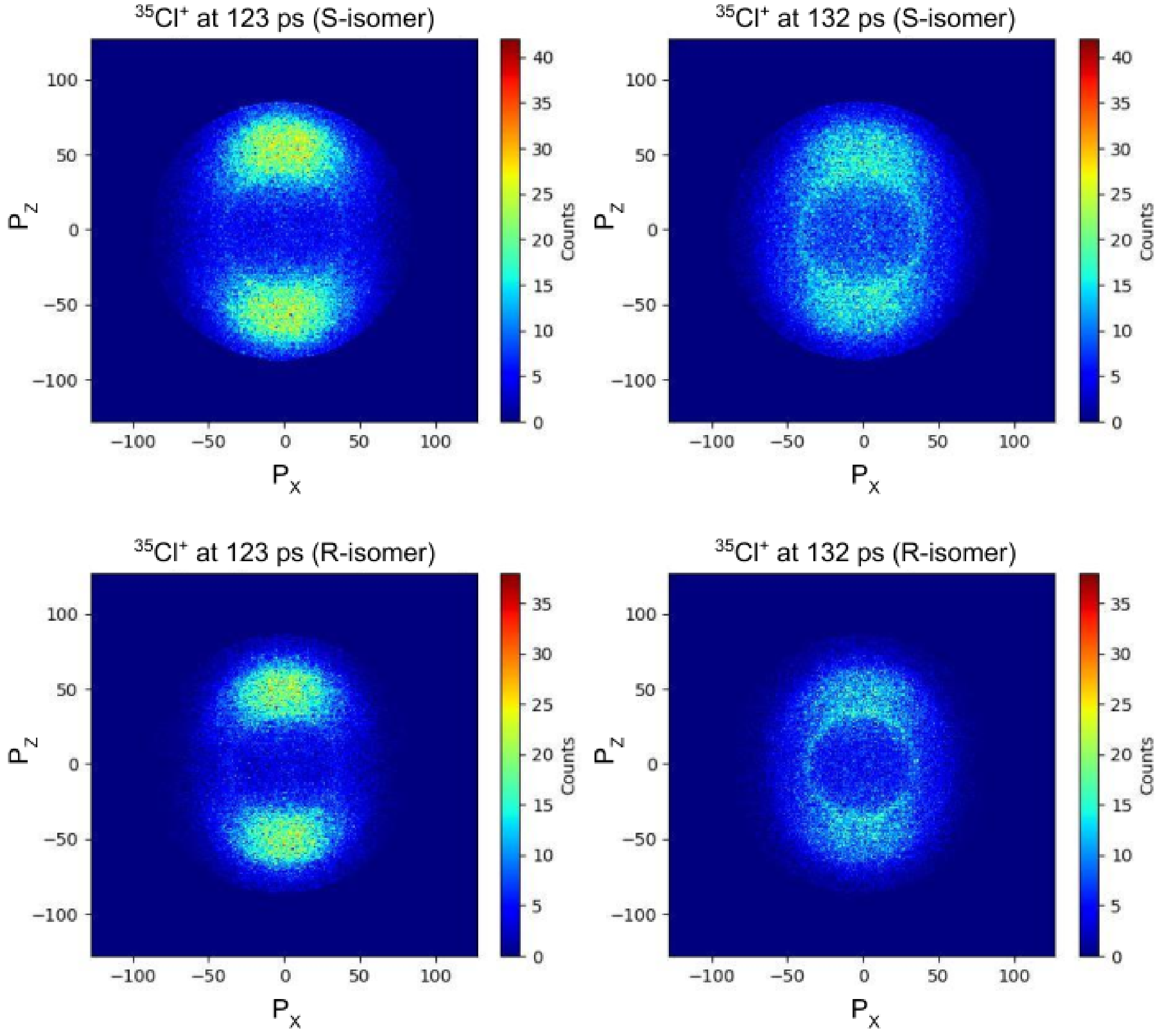

Figure 4.9: *Momentum distributions of* $^{35}Cl^{+}$ *(S-isomer at top, R-isomer at bottom) at the peak and valley of the revival (at time 123 ps and 132 ps after time t0) in arbitrary units.*

Fig 4.10 shows that $C_3H_5O^+$ had little kinetic energy and less spread on the detector compared to Cl^+. Though these plots do show that there is more $C_3H_5O^+$ at time 132 ps rather than earlier at time 123 ps.

At this point, though many plots have been made to study the molecule's rotation and alignment with the laser polarization, a point cannot be made about the rotation around the

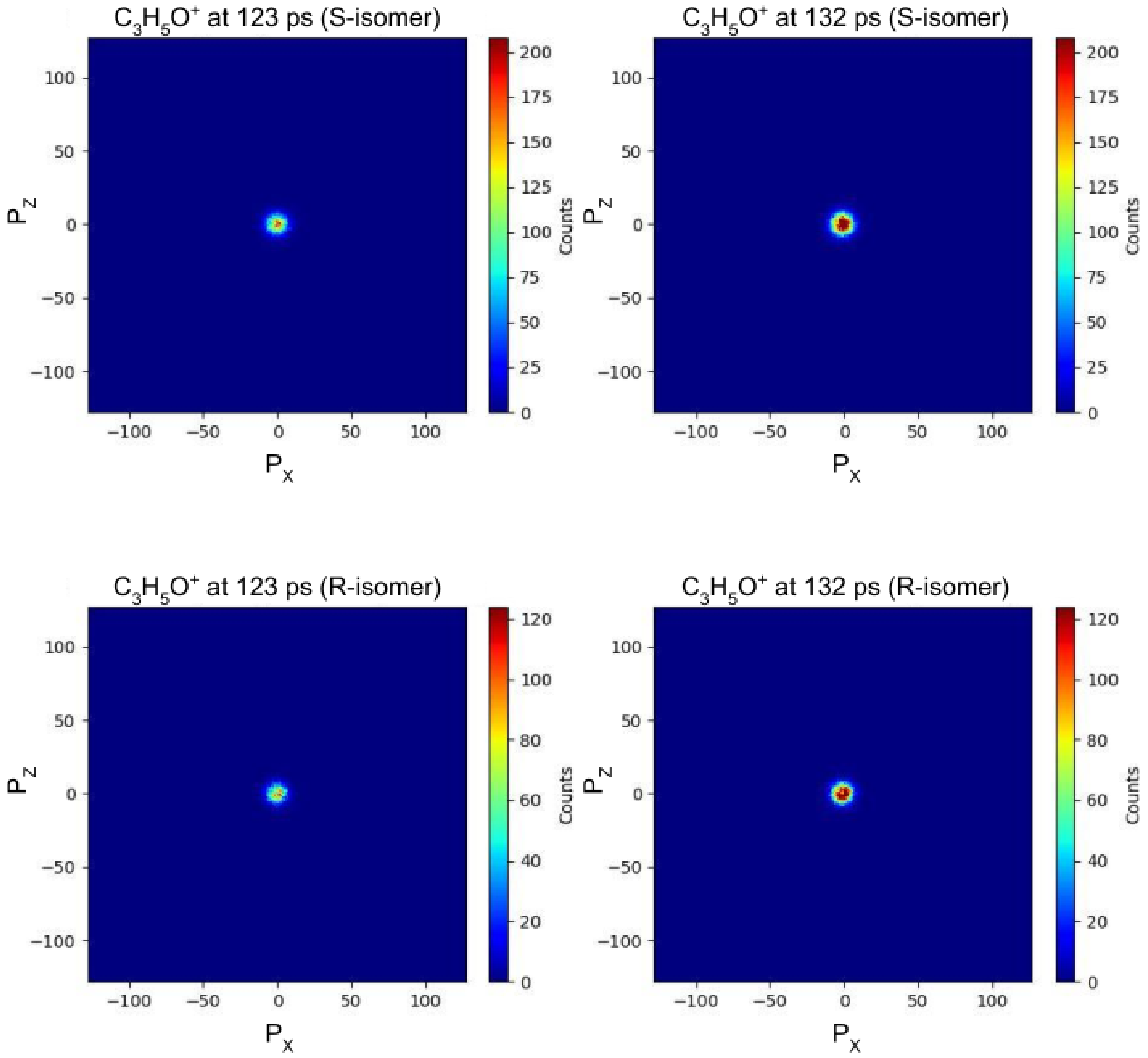

Figure 4.10: *Momentum distributions of $C_3H_5O^+$ (S-isomer at top, R-isomer at bottom) at the valley and peak of a revival (at time 123 ps and 132 ps after time t0) in arbitrary units.*

molecular z axis. One way to study this motion is to look at the angle distribution regarding where the O^+ ions fly off. However, as shown in Fig 4.3, the ion fragments of O^+ are very close and merge with other ions near their TOF, such as CH_2^+. This results in a signal yield and momentum plots that cannot be identified as solely O^+ fragments, and therefore cannot be used to make any statement about this type of motion.

Chapter 5

Conclusion and Outlook

A pump-probe experiment was conducted to drive the chiral epichlorohydrin molecule to rotate and ionize it into fragments. From these fragments, we could study what the orientation of the molecule was in the moment before it was fragmented.

One question we wanted to investigate was whether and how the motions of our chiral molecule changed when comparing one isomer to the other. For both isomers, the pump pulse induced rotational motion of the molecule's most polarizable axis and caused the alignment and misalignment with the polarization of the laser. We see from our figures in Chapter 4 that we can use the normalized signal yield as a reference for these revivals. However, results have not yet shown any difference between the rotation about the molecule's most polarizable axis. Perhaps this difference can be found from other pairs of pump-probe intensities.

In the future, this experiment can also be redone with a higher intensity of the probe pulse. Epicholorhydrin aligns well for a molecule with no symmetry; however, most ions do not show any angular dependence in the momentum distribution from the plots in Chapter 4. With a more intense probe pulse, the molecule would ionize and fragment faster, and the ions would thus retain memory of the molecular axis distribution.

Our last plotted result at this point is that we can use the normalized signal yield as a proxy for the alignment. However, with the signal yield, we can return back to Eq 2.6. By solving the Schrodinger equation for its wavefunction and finding the position of the molecule, $\rho(\theta, \chi, t)$, we can use this and the signal yield, $S_{ion}(t)$, to calculate the probability of the ion at that orientation $(f_{ion}(\theta, \chi, t))$. This calculation can be continued in the future, as at the moment, we only have some preliminary work with the Schrodinger calculations.

In the past year with this project, we have streamlined the way we collect data with the Timepix3 camera. The electronic and digital setup shown in Fig 3.5 has been updated to allow us to have all of our necessary gathered information directly from the Timepix3 camera. This saves time and storage space to identify synchronization between the external equipment of the chopper and the gas jet. All the plots created in Chapter 4 were made from Python code and from an .hdf5 file, where information of every ion was stored. Future analyses can be continued by editing the Python scripts.

Bibliography

[1] V. Makhija. *Laser-induced rotational dynamics as a route to molecular frame measurements*. PhD thesis, Kansas State University, Manhattan, KS, 2014.

[2] Amsterdam Scientific Instruments. Amsterdam Scientific Instruments (ASI) — Technology — amscins.com. `https://amscins.com/resources/technology/`, 2025.

[3] A. Zhao, M. V. Beuzekom, B. Bouwens, D. Byelov, I. Chakaberia, C. Cheng, E. Maddox, A. Nomerotski, P. Svihra, J. Visser, V. Vrba, and T. Weinacht. Coincidence velocity map imaging using tpx3cam, a time stamping optical camera with 1.5 ns timing resolution. *Review of Scientific Instruments*, 88(11):113104, 2017. ISSN 0034-6748. doi: 10.1063/1.4996888. URL `https://doi.org/10.1063/1.4996888`.

[4] A. Nomerotski. Imaging and time stamping of photons with nanosecond resolution in timepix based optical cameras. *Nuclear Instruments and Methods in Physics Research Section A: Accelerators, Spectrometers, Detectors and Associated Equipment*, 937:26–30, 2019. ISSN 0168-9002. doi: https://doi.org/10.1016/j.nima.2019.05.034. URL `https://www.sciencedirect.com/science/article/pii/S0168900219306667`.

[5] G. H. C. New. The generation of ultrashort laser pulses. *Reports on Progress in Physics*, 46(8):877, 1983. doi: 10.1088/0034-4885/46/8/001. URL `https://dx.doi.org/10.1088/0034-4885/46/8/001`.

[6] H. Stapelfeldt and T. Seideman. Colloquium: Aligning molecules with strong laser pulses. *Rev. Mod. Phys.*, 75:543–557, 2003. doi: 10.1103/RevModPhys.75.543. URL `https://link.aps.org/doi/10.1103/RevModPhys.75.543`.

[7] T. Seideman. Revival structure of aligned rotational wave packets. *Phys. Rev. Lett.*, 83:

4971–4974, 1999. doi: 10.1103/PhysRevLett.83.4971. URL https://link.aps.org/doi/10.1103/PhysRevLett.83.4971.

[8] H. V. S. Lam, A. S. Venkatachalam, S. Bhattacharyya, K. Chen, K. Borne, E. Wang, R. Boll, T. Jahnke, V. Kumarappan, A. Rudenko, and D. Rolles. Differentiating three-dimensional molecular structures using laser-induced coulomb explosion imaging. *Phys. Rev. Lett.*, 132:123201, 2024. doi: 10.1103/PhysRevLett.132.123201. URL https://link.aps.org/doi/10.1103/PhysRevLett.132.123201.

[9] H. Q. Pham and M. J. Marks. *Epoxy Resins*. John Wiley Sons, Ltd, 2005. ISBN 9783527306732. doi: https://doi.org/10.1002/14356007.a09_547.pub2. URL https://onlinelibrary.wiley.com/doi/abs/10.1002/14356007.a09_547.pub2.

[10] Pubchem compound summary for cid 7835, epichlorohydrin. https://pubchem.ncbi.nlm.nih.gov/compound/Epichlorohydrin.

[11] H. V. S. Lam. *Molecular-frame measurements of light-induced processes using rotational coherences driven by ultrafast laser pulses*. PhD thesis, Kansas State University, Manhattan, KS, 2021.

[12] X. Ren. *Laser-driven rotational dynamics of gas-phase molecules: control and applications*. PhD thesis, Kansas State University, Manhattan, KS, 2013.

[13] R. Trebino, K. W. DeLong, D. N. Fittinghoff, J. N. Sweetser, M. A. Krumbügel, B. A. Richman, and D. J. Kane. Measuring ultrashort laser pulses in the time-frequency domain using frequency-resolved optical gating. *Review of Scientific Instruments*, 68 (9):3277–3295, 1997. ISSN 0034-6748. doi: 10.1063/1.1148286. URL https://doi.org/10.1063/1.1148286.

[14] D. H. Levy. The spectroscopy of very cold gases. *Science*, 214(4518):263–269, 1981. doi: 10.1126/science.214.4518.263. URL https://www.science.org/doi/abs/10.1126/science.214.4518.263.

[15] L. D. Carr, D. DeMille, R. V. Krems, and J. Ye. Cold and ultracold molecules: science, technology and applications. *New Journal of Physics*, 11(5):055049, 2009. doi: 10.1088/1367-2630/11/5/055049. URL https://dx.doi.org/10.1088/1367-2630/11/5/055049.

[16] F. Wang and P. L. Polavarapu. Conformational stability of (+)-epichlorohydrin. *The Journal of Physical Chemistry A*, 104(26):6189–6196, 2000. doi: 10.1021/jp000757c. URL https://doi.org/10.1021/jp000757c.

[17] U. Even. "The Even-Lavie valve as a source for high intensity supersonic beam". *EPJ Techniques and Instrumentation*, 2, 12 2015. doi: 10.1140/epjti/s40485-015-0027-5.

[18] A. T. J. B. Eppink and D. H. Parker. Velocity map imaging of ions and electrons using electrostatic lenses: Application in photoelectron and photofragment ion imaging of molecular oxygen. *Review of Scientific Instruments*, 68(9):3477–3484, 1997. ISSN 0034-6748. doi: 10.1063/1.1148310. URL https://doi.org/10.1063/1.1148310.

[19] J. Ladislas Wiza. Microchannel plate detectors. *Nuclear Instruments and Methods*, 162(1):587–601, 1979. ISSN 0029-554X. doi: https://doi.org/10.1016/0029-554X(79)90734-1. URL https://www.sciencedirect.com/science/article/pii/0029554X79907341.

[20] H. V. S. Lam, S. Yarlagadda, A. Venkatachalam, T. N. Wangjam, R. K. Kushawaha, C. Cheng, P. Svihra, A. Nomerotski, T. Weinacht, D. Rolles, and V. Kumarappan. Angle-dependent strong-field ionization and fragmentation of carbon dioxide measured using rotational wave packets. *Phys. Rev. A*, 102:043119, Oct 2020. doi: 10.1103/PhysRevA.102.043119. URL https://link.aps.org/doi/10.1103/PhysRevA.102.043119.

[21] Y. Wada and R. W. Kiser. Electron impact spectroscopy of some substituted oxiranes1. *The Journal of Physical Chemistry*, 66(9):1652–1657, 1962. doi: 10.1021/j100815a021. URL https://doi.org/10.1021/j100815a021.

[22] L. Holmegaard, S. S. Viftrup, V. Kumarappan, C. Z. Bisgaard, H. Stapelfeldt, E. Hamilton, and T. Seideman. Control of rotational wave-packet dynamics in asymmetric top molecules. *Phys. Rev. A*, 75:051403, 2007. doi: 10.1103/PhysRevA.75.051403. URL https://link.aps.org/doi/10.1103/PhysRevA.75.051403.

[23] Y. Endo and T. Momose. Ftmw spectroscopy of epichlorohydrin: Detection of three conformers. *Journal of Molecular Spectroscopy*, 372:111348, 2020. ISSN 0022-2852. doi: https://doi.org/10.1016/j.jms.2020.111348. URL https://www.sciencedirect.com/science/article/pii/S0022285220301168.

[24] P. M. Felker. Rotational coherence spectroscopy: studies of the geometries of large gas-phase species by picosecond time-domain methods. *The Journal of Physical Chemistry*, 96(20):7844–7857, 1992. doi: 10.1021/j100199a005. URL https://doi.org/10.1021/j100199a005.